





**UNIVERSIDAD DE INVESTIGACIÓN DE TECNOLOGÍA  
EXPERIMENTAL YACHAY**

**Escuela de Ciencias Químicas e Ingeniería**

**TÍTULO: Advanced few Layers Graphene Nanoplatelets - Based  
Electrodes with Enhanced Electrocatalytic Activity for  
Oxygen Reduction Reaction**

Trabajo de integración curricular presentado como requisito para la  
obtención del título de Química

**Autor:**

Briones Macías Mayra Lissette

**Tutor:**

Zamora Ledezma Camilo, Ph.D

**Co-tutor:**

Suppan Flores Gottfried, Ph.D

Urcuquí, Octubre 2020



**SECRETARÍA GENERAL**  
**(Vicerrectorado Académico/Cancillería)**  
**ESCUELA DE CIENCIAS QUÍMICAS E INGENIERÍA**  
**CARRERA DE QUÍMICA**  
**ACTA DE DEFENSA No. UITEY-CHE-2020-00058-AD**

A los 15 días del mes de octubre de 2020, a las 12:00 horas, de manera virtual mediante videoconferencia, y ante el Tribunal Calificador, integrado por los docentes:

<b>Presidente Tribunal de Defensa</b>	Dra. HIDALGO BONILLA, SANDRA PATRICIA , Ph.D.
<b>Miembro No Tutor</b>	Dr. CAETANO SOUSA MANUEL , Ph.D.
<b>Tutor</b>	Dr. ZAMORA LEDEZMA , CAMILO , Ph.D.

El(la) señor(ita) estudiante **BRIONES MACIAS, MAYRA LISSETTE**, con cédula de identidad No. **1313281196**, de la **ESCUELA DE CIENCIAS QUÍMICAS E INGENIERÍA**, de la Carrera de **QUÍMICA**, aprobada por el Consejo de Educación Superior (CES), mediante Resolución **RPC-SO-39-No.456-2014**, realiza a través de videoconferencia, la sustentación de su trabajo de titulación denominado: **ADVANCED FEW LAYERS GRAPHENE NANOPATELETS-BASED ELECTRODES WITH ENHANCED ELECTROCATALYTIC ACTIVITY FOR OX:YGEN REDUCTION REACTION**, previa a la obtención del título de **QUÍMICO/A**.

El citado trabajo de titulación, fue debidamente aprobado por el(los) docente(s):

<b>Tutor</b>	Dr. ZAMORA LEDEZMA , CAMILO , Ph.D.
--------------	-------------------------------------

Y recibió las observaciones de los otros miembros del Tribunal Calificador, las mismas que han sido incorporadas por el(la) estudiante.

Previamente cumplidos los requisitos legales y reglamentarios, el trabajo de titulación fue sustentado por el(la) estudiante y examinado por los miembros del Tribunal Calificador. Escuchada la sustentación del trabajo de titulación a través de videoconferencia, que integró la exposición de el(la) estudiante sobre el contenido de la misma y las preguntas formuladas por los miembros del Tribunal, se califica la sustentación del trabajo de titulación con las siguientes calificaciones:

Tipo	Docente	Calificación
Tutor	Dr. ZAMORA LEDEZMA , CAMILO , Ph.D.	10,0
Presidente Tribunal De Defensa	Dra. HIDALGO BONILLA, SANDRA PATRICIA , Ph.D.	10,0
Miembro Tribunal De Defensa	Dr. CAETANO SOUSA MANUEL , Ph.D.	9,9

Lo que da un promedio de: **10 (Diez punto Cero)**, sobre 10 (diez), equivalente a: **APROBADO**

Para constancia de lo actuado, firman los miembros del Tribunal Calificador, el/la estudiante y el/la secretario ad-hoc.

Certifico que *en cumplimiento del Decreto Ejecutivo 1017 de 16 de marzo de 2020, la defensa de trabajo de titulación (o examen de grado modalidad teórico práctica) se realizó vía virtual, por lo que las firmas de los miembros del Tribunal de Defensa de Grado, constan en forma digital.*

**BRIONES MACIAS, MAYRA LISSETTE**  
**Estudiante**

SANDRA PATRICIA  
HIDALGO BONILLA

Firmado digitalmente por SANDRA  
PATRICIA HIDALGO BONILLA  
Fecha: 2020.10.15 15:43:07 -05'00'

Dra. HIDALGO BONILLA, SANDRA PATRICIA , Ph.D.  
**Presidente Tribunal de Defensa**

Dr. ZAMORA LEDEZMA , CAMILO , Ph.D.  
**Tutor**



Firmado electrónicamente por:

**CAMILO  
ZAMORA**

Dr. CAETANO SOUSA MANUEL , Ph.D.  
**Miembro No Tutor**

MANUEL  
CAETANO  
SOUSA

Digitally signed by  
MANUEL CAETANO  
SOUSA  
Date: 2020.10.15  
16:58:20 -05'00'

CIFUENTES TAFUR, EVELYN CAROLINA  
**Secretario Ad-hoc**



Firmado electrónicamente por:

**EVELYN CAROLINA  
CIFUENTES TAFUR**



## AUTORÍA

Yo, **Mayra Lissette Briones Macías**, con cédula de identidad 1313281196, declaro que las ideas, juicios, valoraciones, interpretaciones, consultas bibliográficas, definiciones y conceptualizaciones expuestas en el presente trabajo; así como, los procedimientos y herramientas utilizadas en la investigación, son de absoluta responsabilidad de el/la autora (a) del trabajo de integración curricular. Así mismo, me acojo a los reglamentos internos de la Universidad de Investigación de Tecnología Experimental Yachay.

Urcuquí, octubre 2020.



---

Mayra Lissette Briones Macías

CI: 1313281196

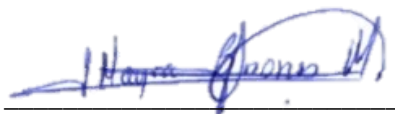


## AUTORIZACIÓN DE PUBLICACIÓN

Yo, **Mayra Lissette Briones Macías**, con cédula de identidad 1313281196, cedo a la Universidad de Investigación de Tecnología Experimental Yachay, los derechos de publicación de la presente obra, sin que deba haber un reconocimiento económico por este concepto. Declaro además que el texto del presente trabajo de titulación no podrá ser cedido a ninguna empresa editorial para su publicación u otros fines, sin contar previamente con la autorización escrita de la Universidad.

Asimismo, autorizo a la Universidad que realice la digitalización y publicación de este trabajo de integración curricular en el repositorio virtual, de conformidad a lo dispuesto en el Art. 144 de la Ley Orgánica de Educación Superior

Urcuquí, octubre 2020.



---

Mayra Lissette Briones Macías

CI: 1313281196



## Agradecimiento

Este trabajo y todo el esfuerzo puesto durante estos cinco años está dedicado a mi familia, por apoyarme, seguirme, aguantarme y nunca perder la fe en mí durante todo el camino, a mi mamá, mi papá, Ary, Dereck y Max, son lo mejor que tengo, siempre estaré en deuda con ustedes. De igual manera, nada de esto lo pudiera haber realizado si no fuese por mis amigos, conocerlos será algo por lo que estaré agradecida por siempre, gracias por apoyarme y literalmente aguantarme en mis buenos y malos momentos, es probable que sin su aguante y empuje no hubiese llegado donde estoy. Nico, Eve, Pau, Kevin, Raúl, Alex y todos los demás que se han ganado un lugar en mí, siempre. Lleva una mención importante al club de fútbol de la universidad y todas las personas que me han permitido ser parte de un equipo sin el que no hubiese podido vivir.

Un gran agradecimiento a la Universidad Yachay Tech, la cual es un gran proyecto que me abrió las puertas a un universo con muchas más cosas de las que pensaba, que te hace expandir la mente para trabajar y ser mejor. Agradezco también a todos los profesores que he tenido a lo largo de estos cinco años, porque ellos son la base de todo, he tenido la suerte de tener excelentes profesores que no solo se preocupan por la excelencia académica, sino también de hacerte una mejor persona y aconsejarte cuando lo necesitas, profe Sandra H., Francisco A., A. Acosta, Javier G., Juan Pablo S., y muchos más. Finalmente, agradecerles a Esteban y a Camilo Z. por haberme ayudado con la tesis, compartiendo conmigo su conocimiento, tiempo y paciencia; y por supuesto a mi tutor Gottfried Suppan, a quien le agradezco, además de ser un excelente profesor, el hecho de haberme acogido como tesista, apoyado, aguantado y tenido una paciencia extraordinaria, por todo esto le estaré agradecida siempre.

Mayra Lissette Briones Macías



## Resumen

Con el fin de estudiar la actividad electrocatalítica que tiene un electrodo hacia la reacción de reducción de oxígeno (RRO), diferentes composiciones de grafeno, fluoruro de polivinilideno y alcohol polivinílico fueron estudiados. Las técnicas de voltametría cíclica y la espectroscopía de impedancia electroquímica fueron utilizadas para determinar la composición de reactivos necesaria para obtener el mejor desempeño en términos de corriente generada, potencial de separación de picos e impedancia, así como también para determinar qué composito tiene la mayor actividad electrocatalítica hacia la reacción de reducción de oxígeno. El composito con 0.4% grafeno / 0.5% PVDF / 0.5% PVA mostró el mejor funcionamiento en cada método, con un pico de corriente catódico de  $-132.7 \mu\text{A}$ , resultado que es 2.1 veces mayor que el de la matriz polimérica y 6.7 veces mayor que la generada por el PVA. El composito también mostró el menor potencial de separación de picos con un valor de 0.17 V y la menor resistencia de transferencia de carga con un valor de  $468.5 \Omega$ , el cual es 4.7 veces menor al valor de la matriz polimérica. Los resultados en cuanto a actividad catalítica mostraron la misma tendencia, con el composito de 0.4% grafeno teniendo la mayor corriente generada a cada pH (el pH toma los valores de 2, 4, 6, 8 y 10) y los valores de onset potential más positivos de  $-0.15 \text{ V vs Ag/AgCl}$  a pH = 2 y  $-0.24 \text{ V}$  a pH = 10, con los menores overpotentials de  $-1.04$  y  $-0.66 \text{ V vs ENH}$  (Electrodo Natural de Hidrógeno) respectivamente, mostrando la mejor actividad electrocatalítica hacia la reacción de reducción de oxígeno.

**Palabras Clave:** Potencial de inicio, pico de corriente catódico, catalizador, RRO.



## Abstract

In order to study the electrocatalytic activity towards oxygen reduction reaction (ORR) of an electrode, different compositions of graphene, polyvinylidene fluoride (PVDF) and polyvinyl alcohol (PVA) were tested. Cyclic voltammetry and electrochemical impedance spectroscopy were used in order to determine the composition of the reagents with the best performance in terms of current generated, potential peak separation and impedance, as well as to determine which composite had the highest electrocatalytic activity towards oxygen reduction reaction. The composite with 0.4 wt% graphene / 0.5 wt% PVDF / 0.5 wt% PVA showed the best performance in each method, with a cathodic peak current of  $-132.7 \mu\text{A}$ , result that is 2.1 times higher than that of the polymeric mixture and 6.7 times higher than the PVA by itself. This composite also showed the lowest potential peak separation of 0.17 V and the lowest charge transfer resistance of  $468.5 \Omega$ , which is 4.7 times lower than that of the polymeric matrix. The results for the catalytic activity demonstrate the same tendency, with the 0.4% composite having the highest current generated at every pH (pH taking the values of 2, 4, 6, 8 and 10) and the more positive values of onset potential of  $-0.15 \text{ V}$  vs Ag/AgCl at pH = 2 and  $-0.24 \text{ V}$  at pH = 10, with the lowest overpotential of  $-1.04$  and  $-0.66 \text{ V}$  vs NHE (Normal Hydrogen Electrode) respectively, showing the best electrocatalytic activity towards oxygen reduction reaction.

**Keywords:** Onset potential, cathodic peak current, catalyst, ORR.

# Contents

<b>List of Figures</b>	<b>iii</b>
<b>List of Tables</b>	<b>iv</b>
<b>1. Chapter 1</b>	<b>1</b>
1.1. Introduction . . . . .	1
1.2. Objectives . . . . .	3
1.2.1. General . . . . .	3
1.2.2. Specifics . . . . .	3
<b>2. Theoretical Background</b>	<b>4</b>
2.1. Oxygen Reduction Reaction . . . . .	4
2.1.1. Kinetics of Oxygen Reduction Reaction . . . . .	6
2.1.2. Catalysts . . . . .	8
2.1.3. Applications . . . . .	12
2.2. Spectroscopic Characterization Techniques . . . . .	15
2.2.1. Raman Spectroscopy . . . . .	15
2.3. Electrochemical Characterization Techniques . . . . .	17
2.3.1. Cyclic Voltammetry . . . . .	17
2.3.2. Electrochemical Impedance Spectroscopy . . . . .	19
<b>3. Methodology</b>	<b>22</b>
3.1. Preparation of Composites . . . . .	22
3.1.1. Reagents and Solutions . . . . .	22
3.1.2. Experimental Procedure . . . . .	22
3.2. Electrochemical Cell Design & Electrode Modification . . . . .	23
3.3. Electrochemical Characterization . . . . .	25
3.3.1. Cyclic Voltammetry . . . . .	25
3.3.2. Electrochemical Impedance Spectroscopy . . . . .	26
<b>4. Results and Discussion</b>	<b>27</b>
4.1. Spectroscopic Characterization . . . . .	27
4.2. Thin Layer Optimization . . . . .	29
4.2.1. Cyclic Voltammetry . . . . .	29
4.2.2. Electrochemical Impedance Spectroscopy . . . . .	35
4.3. Catalytic Activity towards ORR . . . . .	43
<b>5. Conclusion</b>	<b>52</b>

<b>A. Appendix</b>	<b>i</b>
A.1. List of Abbreviations . . . . .	i
A.2. Scientific Output . . . . .	ii
<b>Bibliography</b>	<b>iii</b>

# List of Figures

2.1. Operating principle of a microbial fuel cell . . . . .	13
2.2. Operating principle of a metal air batteries. . . . .	14
2.3. Representation of the Stokes, Anti-Stokes and Rayleigh scattering in Raman spectroscopy . . . . .	16
2.4. Raman spectrum of graphene powder . . . . .	16
2.5. Schematics of the output in cyclic voltammograms . . . . .	17
2.6. Exemplary Nyquist and Bode plots in EIS . . . . .	20
3.1. Electrochemical cell . . . . .	23
3.2. Obtention of a modified electrode . . . . .	25
3.3. Modification of the electrochemical cell and setup for EIS measurements	26
4.1. Raman spectrum for PVDF, PVA, graphene powder and the Gr/PVDF/PVA composite . . . . .	28
4.2. Cyclic voltammograms for the different polymers, polymeric mixture, and composites at different compositions. . . . .	30
4.3. Cyclic voltammograms for the 0.5% PVDF / 0.5% PVA mixture and graphene composites, along with the cathodic and anodic peak currents as a function of graphene content . . . . .	33
4.4. Nyquist plot for all studied composites . . . . .	36
4.5. Randles circuit representation . . . . .	37
4.6. Modified Randles circuit representation . . . . .	38
4.7. Nyquist and Bode plots for the different polymeric matrixes . . . . .	39
4.8. Modified two-parts circuit representation . . . . .	41
4.9. Nyquist and Bode plots for the different graphene/polymers composites	41
4.10. Charge transfer resistance as a function of the amount of graphene of the composite and its improvement. . . . .	42
4.11. Cyclic Voltammetry cathodic measurements for the different composites at different <i>pH</i> values in PBS solutions. . . . .	44
4.12. Onset potential vs. <i>pH</i> and vs. graphene content for all composites. . . .	46
4.13. Contour plot representing the relation between the <i>pH</i> , the graphene content and the overpotential of the composites. . . . .	49
4.14. Onset potential improvements vs. the graphene content at every <i>pH</i> . . .	51

# List of Tables

2.1. Most common circuit elements used in equivalent circuits and its impedance significance. . . . .	21
4.1. Cathodic and anodic peak currents, and peak potential separation of the different composites. . . . .	34
4.2. Polymer and graphene compositions of the different types of composites prepared to be studied as electrodes. . . . .	35
4.3. Equivalent circuit parameters for GC . . . . .	37
4.4. Equivalent circuit parameters for the polymer composites . . . . .	40
4.5. Equivalent circuit parameters for the graphene/polymer composites . .	42
4.6. Cathodic current generated at each composite at -0.6 V vs. Ag/AgCl at different <i>pHs</i> . . . . .	45
4.7. Onset potential and overpotentials for all composites at different <i>pHs</i> . . .	48

# 1. Chapter 1

## 1.1. Introduction

The exponential and alarming growth of population during the past decades and the possibility of reaching over nine billion people by 2050, have created a sense of awareness and concern, leading to an immense field of research opportunities with the investigation of new sources of energy and storage in order to enhance environment control and solve the imminent overpopulation problem <sup>1</sup>.

Solar cells, supercapacitors, batteries, sensors or electrochemical energy storage devices, are some of the most studied possible energy solutions, where electrodes are an essential part of their overall work mechanism. An electrochemical system in which the chemical energy is directly converted to electricity comes as a plausible solution for the global energy demand, and the utilization of common and sustainable materials is the goal to be achieved. In this line, systems such as microbial fuel cells or metal-air batteries, which uses bacteria or transition metals, and oxygen, are quite handy and optimistic.

Oxygen reduction reaction (ORR) is one of the most important mechanisms in energy conversion systems used in different fuel cells. It requires the presence of oxygen by an external flux or by direct contact, and a material that possesses a high catalytic activity for ORR to be kinetically favorable. In fuel cells, an anodic reaction releases protons and electrons that travel, in the case of protons through a membrane or the electrolyte, and in the case of electrons through an external circuit, to the cathode. The cathode is the part of the cell that is in direct contact with oxygen, so by accepting the electrons and protons, a reduction of the oxygen occurs <sup>2,3</sup>, yet it is a kinetically hindered process, with high overpotentials <sup>4</sup>.

## 1. Chapter 1

Platinum is the most common material used as an electrode for ORR, chosen by its ability to increase the velocity of the reaction produced with oxygen, in an efficient manner. Platinum, however, has certain disadvantages like its high cost, the possibility of intoxication with CO<sub>2</sub> and other gases, or the possible biofouling problems<sup>2,5</sup>.

This is the reason why efforts to find affordable materials that conserve or even improve the results of platinum for ORR are made. Some more common metals such as copper, cobalt or iron, have been investigated to replace the high-cost electrodes mentioned before, obtaining results in currents, durability, and tolerance comparable to and, for some of them, better than those of platinum<sup>6-8</sup>. As other possible replacements with metal-free nanoscale carbon electrocatalysts have become a viable option as they have high electrical conductivity, higher surface area, high mechanical strength, durability, and stability in both acidic and basic environments, as well as excellent electrochemical resistance.

The commercial Pt/C catalyst is the common reference because of its great performance towards ORR with a limiting current density of around 6 mA cm<sup>-2</sup> at 1600 rpm. New studied catalysts such as phosphorous doped hierarchical porous carbon show a shift of around 70 mV for the onset potential compared with the Pt/C electrode<sup>9</sup>. Carbon fiber paper with Pt<sub>3</sub>Co showing a limiting current density of 25.8 mA cm<sup>-2</sup> at 2500 rpm<sup>10</sup> and Mn<sub>3</sub>O<sub>4</sub> oxidized graphene flakes nanocomposites gave a limiting current density of 2.8 mA cm<sup>-2</sup> at 1600 rpm<sup>11</sup>, have also been studied.

Graphene is an interesting material, as it has the possibility of becoming a promising alternative to platinum electrodes. Its high surface area, electronic conductivity, electrochemical stability, or the possibility of taking advantage of both sides of its planar structure<sup>12</sup> come in as facilities to be catalytically favorable for ORR. For the correct performance of it as electrode, graphene must be used in a matrix, in this case, a polymeric one, which allows conductivity but does not react.

This work will contribute to understanding the relationship between the chemical

## *1.2. Objectives*

makeup of a nanocarbon modified electrode and its catalytic activity towards ORR. For this purpose, composite electrodes based on graphene will be prepared and characterized through Raman spectroscopy and electrochemical methods, such as cyclic voltammetry and electrochemical impedance spectroscopy.

## **1.2. Objectives**

### **1.2.1. General**

Development of graphene-based electrodes acting as a catalyst to achieve high electrocatalytic activity towards oxygen reduction reaction.

### **1.2.2. Specifics**

- Modification of the surface of a glassy carbon electrode with different graphene-polymer composites.
- Characterization of the composite electrodes by Raman Spectroscopy.
- Characterization of composite electrodes by Cyclic Voltammetry and Electrochemical Impedance Spectroscopy.
- Evaluation of the electrocatalytic activity of the electrodes under different conditions.

## 2. Theoretical Background

### 2.1. Oxygen Reduction Reaction

The oxygen reduction reaction is a very essential mechanism as it is the pathway used by organisms for respiration. Working similarly, ORR is also highly investigated by its use in energy converting systems like fuel cells or metal-air batteries. Most of these different systems work with a cathode in which an ORR is performed. It can happen by introducing the cathode into a solution and enabling O<sub>2</sub> to diffuse to it, or by placing the cathode in direct contact with air.

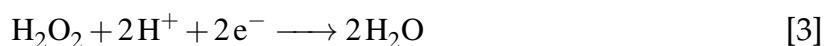
However, this process still faces great challenges such as a slow reaction rate due to poor kinetics of ORR, the high overpotential of oxygen reduction on the surface of the cathode at neutral *pH*, or the reduced contact between oxygen and the cathode material itself<sup>13</sup>. Several different approaches have been proposed to improve the performance of the cathode: attempts to lower the reaction overpotential with the use of mediators, electrode modification with catalysts, and optimizing operational conditions within the cathodic compartment have been mentioned in the literature<sup>2</sup>.

Normally, the ORR mechanism in aqueous media proceeds either by a four-electron or by a two-electron transfer process, mostly depending on the type of catalyst used,<sup>14</sup> while the latter is important in hydrogen peroxide production, shown by reaction [2], the four-electron transfer (shown in reactions [1] and [4]) is preferable for fuel cells. Moreover, the four-electron ORR process is observed to be more dominant if noble-metal based electrocatalysts are used, whereas carbon nanomaterials-based electrocatalysts, transition metal oxides, and hybrid nanomaterials may facilitate the ORR mechanism via two-electron transfer or via a combination of both<sup>15</sup>.

## 2.1. Oxygen Reduction Reaction

It has been studied that the  $pH$  of the medium strongly affects the catalytic pathways<sup>4</sup>, with different types of chemical reactions associated with each. In the four-electron ORR process (shown in reactions [1] and [4]), oxygen directly reduces to water, while in the two-electron ORR process shown in reactions [2] and [5], oxygen reduces to an intermediate that can be reduced later as shown in reactions [3] and [6]. Both acidic and basic reaction mediums are listed below<sup>16</sup>.

Acidic aqueous solution:



For reactions [1] to [3], the thermodynamic electrode potentials at standard conditions are 1.23 V, 0.70 V, and 1.76 V vs. NHE, respectively.

In an alkaline aqueous solution, the corresponding reactions become:



## 2. Theoretical Background

And for reactions [4] to [6], the thermodynamic electrode potentials at standard conditions are of 0.401 V, -0.065 V, and 0.867 V vs. NHE, respectively.

There are some catalysts which are incapable of reducing the H<sub>2</sub>O<sub>2</sub> to H<sub>2</sub>O at sufficient rates, so the reduction process will end after the first two electron reduction steps, finishing in reaction [2]. In this case, the 2-electron pathway produces H<sub>2</sub>O<sub>2</sub> as an intermediate or the end product of the oxygen reduction, causing degradation of the cathode catalysts and leading to a high overpotential <sup>2</sup>.

The material with the best known electrocatalytic performance for ORR is platinum, presenting a high activity and durability in acidic media, even though the reduction of the oxygen rate is from over five orders of magnitude slower than that occurring in the anode for hydrogen oxidation in the case of proton exchange membrane (PEM) fuel cells <sup>12</sup>. This example shows the sluggish kinetics of the reaction and the necessity of improving the catalytic activity of the material used as catalyst. For this reason, different cathode electrocatalysts have been investigated, in the line of precious metal catalysts, especially Pt-based catalysts <sup>17</sup>, or more common and affordable materials containing transition metals or nanocarbons.

### 2.1.1. Kinetics of Oxygen Reduction Reaction

In terms of kinetics, the potential of the ORR should be as close as possible to the thermodynamic electrode potential. If this is not the case, as for ORR, the overpotential of the mechanism is high. Overpotential ( $\eta$ ) is defined as the resultant potential ( $E$ ) minus the equilibrium potential ( $E_{eq}$ ), <sup>18</sup> as shown in Reaction 2.1, the higher this value, the slower the kinetics of the reaction.

$$\eta = E - E_{eq} \quad (2.1)$$

This obtained overpotential is a sum of different contributions as shown in equation

## 2.1. Oxygen Reduction Reaction

2.2, where  $\eta_a$  is the activation overpotential,  $\eta_c$  the concentration overpotential, and  $iR$  the ohmic drop, which entails contributions from charge transfer, mass transport and electrolytic resistivity from the overall electrochemical setup of the process.

$$\eta = \eta_a + \eta_c + iR \quad (2.2)$$

The relation between the overpotential and the current is given by the Butler-Volmer equation (2.3) where  $j$  is the ORR current density,  $j_0$  is the exchange current density,  $n$  is the number of electrons transferred in the rate-determining step,  $\alpha$  is the transfer coefficient,  $\eta$  the overpotential defined in equation 2.1,  $F$  the Faraday constant,  $R$  the gas constant and  $T$  the temperature in Kelvin.

$$j(\eta) = j_0 \left( e^{\frac{\alpha n F \eta}{RT}} - e^{\frac{(1-\alpha) n F \eta}{RT}} \right) \quad (2.3)$$

To generate high current densities, when a low overpotential occurs, the exchange current density should be large or  $RT/\alpha n F$  small<sup>16</sup>. ORR often occurs at high overpotentials, so the Butler-Volmer equation becomes the Tafel equation that will be further discussed in Section 2.2.1.

The relation between the onset potential and the  $pH$  can be explained by the Nernst equation for a redox reaction (Eq. 2.4), where  $Q$  is the reaction quotient, if the reaction includes as a reagent or as a product  $[H^+]$  or  $[OH^-]$ . In the case of the ORR, depending on the media, the standard potential of the cell and the value of the relation in their activities ( $a(red)/a(ox)$ ) changes (see equation 2.5).

$$E = E^\circ - \frac{RT}{nF} \ln(Q) \quad (2.4)$$

$$E = E^\circ - \frac{RT}{nF} \ln \left( \frac{a(red)}{a(ox)} \right) \quad (2.5)$$

## 2. Theoretical Background

The electrochemical potential as a function of  $pH$  will be further discussed in chapter 4.3.

### 2.1.2. Catalysts

In order to improve the kinetics of ORR, several efforts have been made, especially regarding the material of the catalyst. Even though platinum has shown the best results as a catalyst, it has also shown certain disadvantages such as the possibility of intoxication with other gases, its scarcity problems, which lead to high costs, among others<sup>19</sup>.

For a catalyst to be good, it must have a good electrocatalytic activity towards ORR, an adequate surface, and great interaction and binding affinity with oxygen. In this way, it should have a high number of intrinsic active sites for oxygen to adsorb<sup>16</sup>. As studied by Wu, Yang & Yan<sup>9</sup>, a useful catalyst should have a large surface area, disperse active sites, and places in which solid, liquid, and gas can easily perform mass transfer during ORR.

According to Nørskov *et al.*, the adsorption energy needed for the intermediates of the reaction to adsorb in the surface of platinum catalyst, to have a good catalytic activity towards ORR, has a value of 0.1 eV. Pt electrode shows a slightly higher value, and it is the cause of the high overpotential the reaction presents, and hence the sluggish kinetics<sup>20</sup>. In the next section, a small review of some of the possible materials used as catalysts for ORR and their exceptional characteristics are stated.

#### Platinum and noble metal catalysts

As stated before, platinum is the chosen material for ORR due to its high stability and electrochemical activity, that is why the most used and commercialized catalyst for ORR is Pt nanoparticles supported by high-surface-area carbon. Yet, its disadvantages

## 2.1. Oxygen Reduction Reaction

mainly in cost, make it not sustainable for energy converting systems. Different options to use less raw material involves changes in morphology and size, such as shell core platinum electrodes, or platinum alloy electrodes.

For shell core platinum, the basis is to form several atom layers of Pt surrounding a nanoparticle of cheaper metalcore. The metals could be from Pd, Ru or Re, and there are different techniques for the shell formation, such as electrochemical dealloying, annealing, acid leaching, among others <sup>21</sup>. For them, ORR activity can be enhanced with an appropriated platinum thickness and proper geometry and electronic effects from the subsurface of nanoparticles <sup>22</sup>. Yet, the disadvantages come as its stability can be altered by a non-ideal quantity of Pt present in the shell.

Platinum alloys allow to reduce the platinum quantity necessary for the electrode and can make ORR reach a higher catalytic activity by changing the bond strength of oxygen and oxygen intermediates with the catalyst itself, because of the additional compound. Some of the compounds used as alloys are Pt<sub>3</sub>Ni(111) and Pt<sub>x</sub>Gd NPs, which exhibit higher activity than the known Pt/C electrode <sup>23</sup>. Yet, these alloys can be thermodynamically unstable as they tend to dealloy (dissolve in the electrolyte) and cause degradation.

### **Non-precious metal catalysts**

Pointing to their cost and toxicity, high chemical stability, and catalytic capacity, transition metal oxides have been investigated for possible use as catalysts for energy converting devices, giving the main focus to manganese dioxide (MnO<sub>2</sub>).

Studies have shown that the manner in which MnO<sub>2</sub> is synthesized, its crystal structure, particle size, and the support material determines its catalytic activity with  $\beta$ -MnO<sub>2</sub> as the most effective catalyst with a maximum power density of  $3773 \pm 347$  mW/m<sup>3</sup> but with low electrical conductivity results and poor dispersion <sup>24</sup>. As a method to improve it, this oxide can be incorporated into electron-conductive mate-

## 2. Theoretical Background

rials like nanocarbon.

Wen *et al.* <sup>25</sup> proved that the nano-structured MnO<sub>2</sub>/Graphene Nano Sheets (GNS) composite exhibited an excellent catalytic activity for ORR due to MnO<sub>2</sub> nanoparticles closely anchored on the excellent conductive graphene nanosheets. Co oxides possess a high electrocatalytic activity, which make them a plausible option as catalysts. Co<sub>3</sub>O<sub>4</sub> has the advantage of presenting a crystal structure in which Co<sup>2+</sup> and Co<sup>3+</sup> coexist, providing different types of active sites for ORR <sup>16</sup>.

### **Nano-carbon based catalysts**

Functional carbon-based nanomaterials (CBNs) have become important due to their unique combinations of chemical and physical properties (i.e., thermal and electrical conductivity, high mechanical strength, and optical properties) <sup>26</sup>.

#### **Carbon nanotubes**

Carbon nanotubes (CNTs) have become the most widely used CBNs. They are commonly synthesized by arc discharge or chemical vapor deposition of graphite, with a cylindrical structure, and a wide range of electrical and optical properties based on their extended sp<sup>2</sup> carbon and their physical properties (e.g., diameter, length, single-walled vs. multi-walled, surface functionalization, and chirality) <sup>27</sup>.

Because of its properties, CNTs have been explored for use in many industrial applications. For example, CNTs are well known for their super mechanical strength: their measured rigidity and flexibility are greater than that of some commercially available high-strength materials as high tensile steel or carbon fibers <sup>28</sup>. One of the problems associated with CNTs is their poor interaction with the surroundings matrixes, which results in poor and inefficient load transfer <sup>28</sup>.

Researches have been addressed to incorporate CNTs into other materials to utilize their multi-functional nature. Properties such as its low threshold electric fields, their nanoscale dimension facilities, or its strong luminescence from field emission are used

## 2.1. Oxygen Reduction Reaction

for high-efficiency electron emission devices such as electron microscopes, flat display panels, and gas-discharge tubes or for lighting devices, supercapacitors or batteries <sup>29</sup>.

### **Activated carbon**

Activated carbon (AC), popularly known as activated charcoal or activated coal, is a common material used for different applications in industry. The fine structure possessed by AC increased the surface area ( $>1000 \text{ m}^2 \text{ g}^{-1}$ ) of pores that result in possession of powerful adsorptive properties. Carbon is available in three main forms; these are; powder, granular, and pellet. Nonetheless, the most frequently used are granular and powdered AC. There are other forms of AC, such as fibers, which are mainly obtained from petroleum pitch and isotropic coal, felts, and clothes. The AC is found to be useful in removing many contaminants from both potable water and wastewater as a result of its high surface area <sup>30</sup>.

### **Graphene**

The discovery of graphene by Andre Geim and Konstantin Novoselov in 2004 has motivated the scientific community to explore the potential applications of this material extensively <sup>31</sup>. Graphene is commonly referred to as a two dimensional (2D) sheetlike material with  $sp^2$  hybridized carbon atoms configured in a hexagonal structure with a thickness corresponding to an atom diameter <sup>32</sup>. It is made up of pure carbon, and each carbon atom is covalently bonded together in the same plane, and graphene monolayer sheets forming by linked by van der Waals forces.

Along with its derivatives, particularly graphene oxide (GO) and reduced graphene oxide (rGO), graphene materials have been studied in various fields because of the presence of an aromatic ring, free  $\pi$ - $\pi$  electron, and reactive functional groups <sup>33</sup>. It has outstanding physical, chemical, and electrochemical properties; it can sustain current densities six orders of magnitude higher than that of copper <sup>34</sup>, which is an efficient electrode material for creating new sensing assays due to its large conductivity, fast heterogeneous electron transfer, and large surface area <sup>35</sup>. Graphene-modified elec-

## 2. Theoretical Background

trodes prepared by different methods have been used for the successful determination of various biomolecules with high sensitivity and selectivity in the past few years<sup>2</sup>.

It can be stacked to form 3-D graphite, rolled to form 1-D nanotubes, and wrapped to form 0-D fullerenes. Long-range  $\pi$  conjugation in graphene results in its extraordinary thermal, mechanical, and electrical properties. Graphene is impermeable to gas and liquids, has excellent thermal conductivity and higher current density in comparison to other most effective materials<sup>36</sup>.

So far, graphene-based materials have been extensively investigated and envisaged as potential electrode materials for lithium-ion batteries, supercapacitors, biosensors, photovoltaic cells, and catalysis due to its attractive properties, including high surface area (theoretical value  $2630 \text{ m}^2 \text{ g}^{-1}$ ), high conductivity, and easy synthesis process<sup>37</sup>. Recent studies show the maximum power density of the microbial fuel cells has been significantly improved by using graphene as the catalyst support due to the better dispersion of the metal catalysts on the graphene surface. In addition to being an excellent catalyst support, the potential of using graphene-based cathode/anode electrode has also been demonstrated in some studies<sup>25</sup>.

### 2.1.3. Applications

As stated before, ORR is primordial for energy converting systems such as the different types of fuel cells and metal-air batteries. The cathode in an electrochemical system is the electrode where a reduction reaction is going to occur, and in the cases mentioned above, oxygen is the molecule to be reduced. There are different types of fuel cells like microbial fuel cells (MFCs), proton exchange membrane fuel cells, polymer electrolyte fuel cells, hydrogen fuel cells, among others. In this section, a brief review of MFCs and metal-air batteries will be explained.

## 2.1. Oxygen Reduction Reaction

### Microbial fuel cells

MFCs are devices in which viable microorganisms act as catalysts using organic fuel sources to generate electric energy<sup>19</sup>. The overall setup of a microbial fuel cell consists of an anodic part where bacteria and the different substrates coexist in an anaerobic environment leading to an oxidation reaction and a cathodic section where the electrons and protons released from the anode, react with an electron acceptor compound which is reduced. Figure 2.1 shows a simple schematic of the common setup of an MFC.

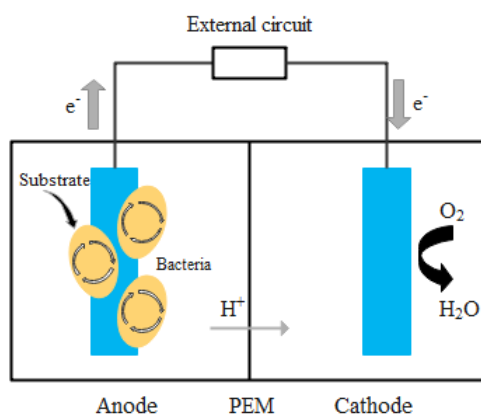


Figure 2.1.: Schematic operating principle of an MFC.

At the cathode, an electron acceptor compound closes the circuit by reducing oxygen to water; this part of the cell is aerobic and can be either an open system in direct contact with air or an oxygen supplied (by an external source) system. For the efficient and correct functioning of MFCs, it is necessary to understand the effects materials of the electrodes have on the overall performance. In the anode, primordial requests are a good conductivity, biocompatibility, and high surface area, characteristics that certain carbon materials like carbon black, graphite, carbon paper, carbon cloth could easily provide<sup>38</sup>. Cathodes, on the other hand, should have a great catalytic activity towards ORR.

The material from which the cathode is composed is directly proportional to the

## 2. Theoretical Background

efficiency of the cell and hence to the final currents generated. In the same manner, the contact area of the electrode has to be the highest possible, as output power is directly relevant to the amount of oxygen in solution <sup>38</sup>.

### Metal-air batteries

In order to improve the performance of lithium-ion batteries in terms of energy and power density, new forms of batteries have been largely studied. In this manner, metal-ion batteries have come as a possible competitor as they are cataloged as high-energy batteries. Figure 2.2 shows the general functioning of this type of cell.

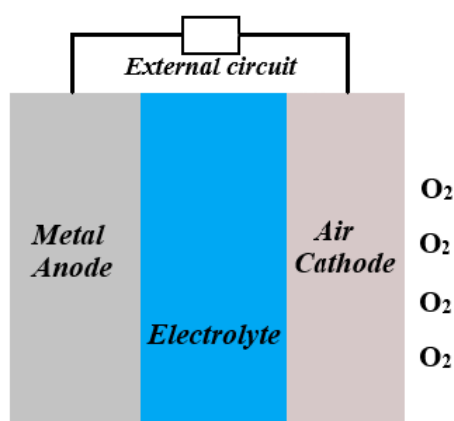


Figure 2.2.: Schematic operating principle of a metal-air battery.

The battery consists of metal oxidation at the anode, an electrolyte, and a cathode which is in direct contact with air to produce an oxygen reduction reaction. As the metal gets oxidized, metal ions are formed and electrons released, traveling through the electrolyte until it reaches the cathode where it reacts with the oxygen reducing it, with the overall process resulting in a high energy density of the device <sup>39</sup>. Different types of metals have been used as cathode naming Li, Na, Al, Mg, Fe, Zn, Fe or Sn from which lithium is the most studied one, showing a large energy density of around  $3456 \text{ Wh Kg}^{-1}$ , higher than that for lithium-ion batteries of  $100\text{--}200 \text{ Wh Kg}^{-1}$  <sup>40</sup>.

## 2.2. Spectroscopic Characterization Techniques

The different type of material used in both electrodes is crucial to determine the final performance of the battery <sup>41</sup>. For the cathodic reaction, not only ORR occurs but oxygen evolution reaction (OER) too, so a material which improves the kinetics of ORR can help to reduce the resistance of mass transport during the overall process and have a specific pore size to prevent the interaction of by-products is needed <sup>42</sup>.

## 2.2. Spectroscopic Characterization Techniques

### 2.2.1. Raman Spectroscopy

Raman spectroscopy is based on the interaction of the light with a sample, yet it is not the absorbed nor the reflected wavelengths that come to matter, but the few scattered radiations which do not have the same wavelength as the others; this phenomenon is known as Raman effect.

Scattered light can be whether Rayleigh or Raman, where in the first one, the elastically scattered photons possess the same energy, wavelength ( $\lambda$ ), and frequency ( $\nu$ ) of the incident photons. Raman scattering on the other side, constitutes the part of the light (1 out of 10<sup>7</sup> photons <sup>43</sup>) which is scattered at different frequencies (most of the times at lower frequencies), oscillating between a specific vibrational frequency of the molecule times from and to the Rayleigh scattering (see Fig. 2.3). These lines of frequencies are the Stokes and anti-Stokes lines in a spectrum. Raman spectroscopy shows then, the obtained vibrational frequency, which changes from the incident beam frequency <sup>44</sup>.

This phenomenon can be associated with a change in the electronic, vibrational, or rotational energy, yet the vibrational effect is the most studied one. The difference between the energy of the incident photon with the scattered photons mentioned before led to the energy of the vibration of the scattered molecule <sup>43</sup>. The common spectrum

## 2. Theoretical Background

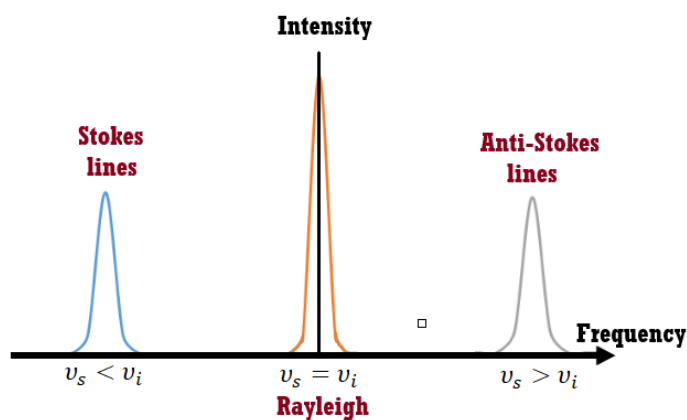


Figure 2.3.: Representation of the Stokes, Anti-Stokes, and Rayleigh scattering in Raman spectroscopy, where  $\nu_i$  is the Rayleigh scattering frequency and  $\nu_s$  is the Raman scattering frequency.

shows the intensity of the scattered light vs. the energy difference).

Among the most common applications of Raman spectroscopy are reaction and environmental monitoring, material chemistry, chromatographic detection, and it has been widely used in the identification of nanomaterials. Its ability to show specific chemical identification and the possibility to use it along with other analytical techniques, assert Raman spectroscopy as a useful technique<sup>43</sup>. In Fig. 2.4 a representation of the Raman spectrum from graphene powder is presented<sup>44</sup>.

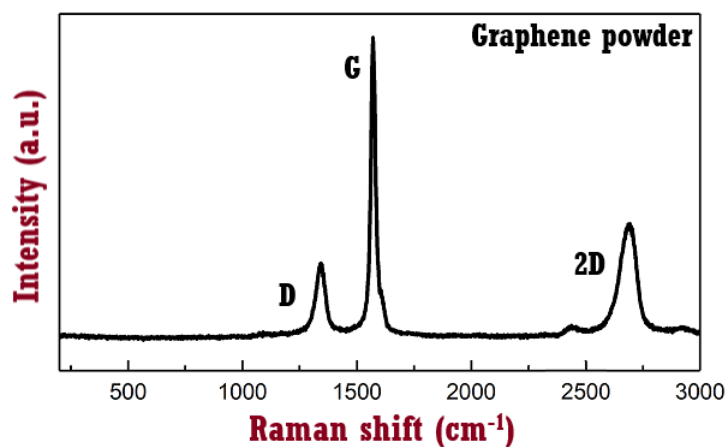


Figure 2.4.: Representation of a Raman spectrum corresponding to graphene powder, with its representative D, G, and 2D bands that will be further studied in section 4.1.

## 2.3. Electrochemical Characterization Techniques

### 2.3.1. Cyclic Voltammetry

Cyclic voltammetry (CV) is a very common electrochemical technique used to investigate the redox processes species can undergo if an external potential is applied and varied with time (see Figure 2.5 b), obtaining the system's response (current)<sup>45</sup>. It can be chosen to study an electrochemical system under different conditions, catalysis electron transfer reactions, intermediates in redox reactions, diffusion coefficients, formal reduction potentials, the reversibility capacity of a system, and concentrations of unknown solutions<sup>46</sup>. Information is presented in a current/current density vs. potential plot similar to a normal spectrum (Figure 2.5 a), giving information of the current at the working electrode as a function of a potential scan<sup>46</sup>.

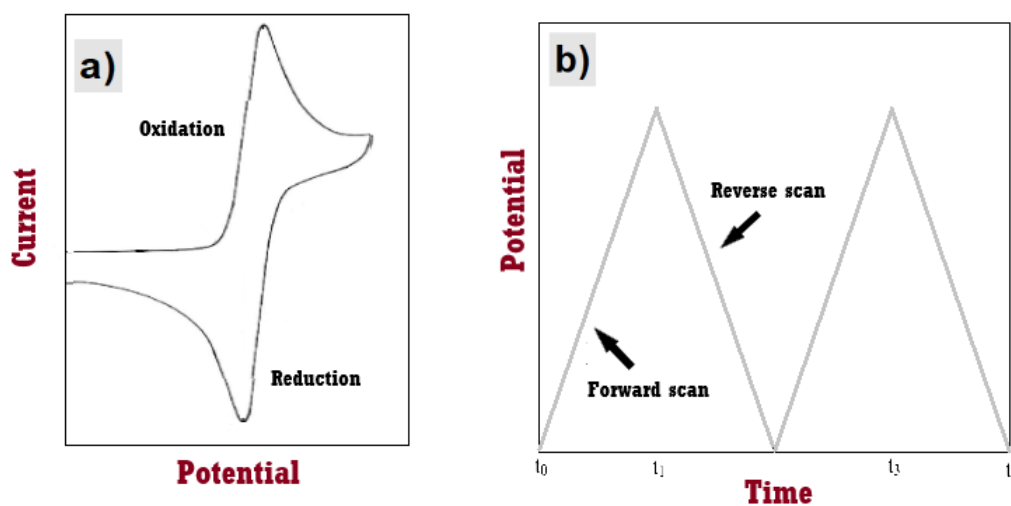


Figure 2.5.: a) Cyclic voltammogram of an electrochemically active, reversible species. b) Potential as a function of time for a cyclic voltammogram, with initial, switching, and end potentials.

It must be comprehended that this technique is set to a more qualitative first approach to experiments. If quantitative results are required, step or pulse techniques are the most plausible solutions<sup>46</sup>. The specialty of CV is its capacity to generate

## 2. Theoretical Background

species during one scan and then probe them with subsequent scans <sup>46</sup>. An electrochemical cell with a three-electrode configuration is used, where an external potential is applied on the working electrode and referenced against a reference electrode. A counter electrode serves as a current collector to complete the electric circuit of the cell.

The cyclic voltammetry peak height,  $i_p$ , is directly proportional to the analyte concentration,  $C$ , as described by the simplified Randles–Sevcik equation (equation 2.6), if the temperature is assumed to be 25 °C:

$$i_p = kn^{3/2}AC_{FC}\sqrt{\nu D} \quad (2.6)$$

In this equation,  $k$  is a constant of  $2.69 \times 10^5 \text{ C mol}^{-1} \text{ V}^{-1/2}$ ,  $n$  is the number of electrons appearing in the half-reaction for the redox couple,  $A$  is the electrode area ( $\text{cm}^2$ ),  $D$  is the analyte diffusion coefficient ( $\text{cm}^2 \text{ s}^{-1}$ ), and  $\nu$  is the rate at which the potential is swept ( $\text{V s}^{-1}$ ).

For quasi reversible and irreversible systems, the electron diffusion coefficients can be obtained from cyclic voltammograms by using a modified Randles–Sevcik equation <sup>47</sup> (equation 2.7):

$$i_{pa} = 0.4961nFAC_o^* \sqrt{\frac{\alpha n F \nu D_E}{RT}} \quad (2.7)$$

Where  $i_{pa}$  denotes the anodic peak current,  $n$  denotes the number of electrons appearing in the redox reaction,  $A$  the surface area of the electrode,  $C_o^*$  the bulk concentration of the redox-active molecules,  $\alpha$  the transfer coefficient of the electrochemical reaction and  $\nu$  the rate at which the potential is swept.

From CVs, different kinds of information can be obtained. The onset potential allows to evaluate the minimum potential needed to start the reaction; it is normally measured first even though an exact value is difficult to obtain because the currents are very low at that point <sup>48</sup>. The half-wave potential is determined by the activity of the catalyst

### 2.3. Electrochemical Characterization Techniques

and, pointing to the reduction of oxygen, for the efficiency of oxygen diffusion at its surface, being the point in which the reaction is controlled by both parts, showing the efficiency of the catalyst <sup>48</sup>.

The limiting current density depends on the speed in which oxygen diffuses to the surface of the catalyst, being influenced by the porosity and the surface of it. For good ORR catalysts, limiting current density is around 5–6 mA cm<sup>-2</sup> <sup>49</sup>. The exchange current density ( $j_0$ ) is the current at zero overpotential (as in equation 2.3), is like a background current that determines the speed of an electrochemical reaction and reflects the analyte/electrode interaction in terms of rates of electron transfer.

To understand the kinetics and mechanism of the reaction, a Tafel analysis is commonly used. This is important because a comparison can be made between different catalysts. The Tafel slope is related to the rate-determining step calculating the current response to the given voltage <sup>50</sup> by using Equation (2.8).

$$\eta = b \cdot \log \left( \frac{j}{j_0} \right) \quad (2.8)$$

where  $\eta$  is the overpotential,  $b$  the Tafel slope,  $j$  the current density, and  $j_0$  the exchange current density. Good catalysts possess small Tafel slope and large current density values.

#### 2.3.2. Electrochemical Impedance Spectroscopy

According to Ohm's law, a resistor is defined as an entity whose value does not change as a function of frequency, and its signals (from current and voltage through it) are in phase. For non-ideal systems in which the previously described is not useful, the relationship between potential and current is called impedance <sup>51</sup>.

Electrochemical impedance spectroscopy (EIS) is a technique based in the application of an alternating potential to a sample which responds with a resultant current

## 2. Theoretical Background

<sup>51</sup>. Impedance ( $Z$ ) is expressed in terms of a magnitude ( $t$ ) and a phase shift ( $\omega$ ) <sup>52</sup> at a particular frequency  $\omega$ , as shown in Equation (2.9).

$$Z(\omega t) = \frac{|E(\omega t)|}{|i(\omega t)|} \quad (2.9)$$

The two most common forms of impedance data presentation are Nyquist plots and Bode plots. The first one shows the imaginary part of the impedance versus the real part <sup>53</sup> and, the latter, the Bode plot, represents the absolute value of the impedance or the phase shift vs. the frequency ( $f$ ), complementing the information given by the Nyquist plots (see Figure 2.6) <sup>51</sup>.

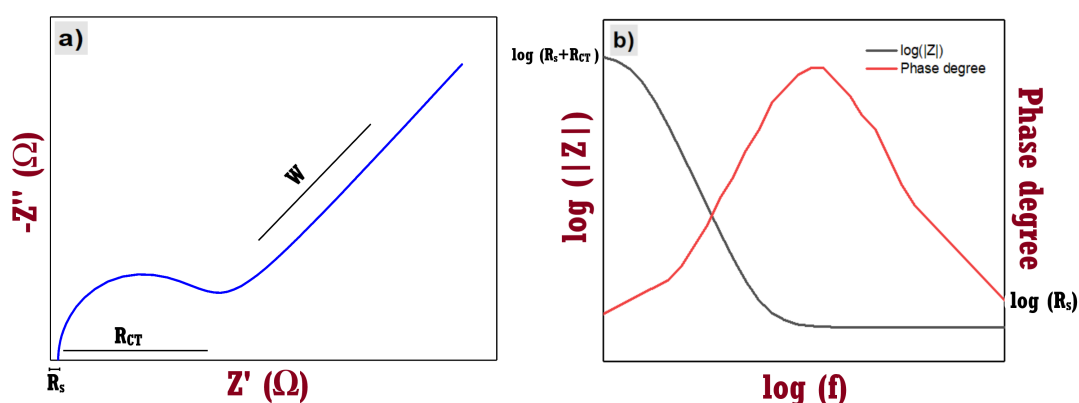


Figure 2.6.: Exemplary a) Nyquist and b) Bode plot obtained from electrochemical measurements.  $R_s$  is the solution resistance,  $R_{CT}$  is the charge transfer resistance and  $W$  is the Warburg resistance.

Some of the applications of EIS are to probe several electrochemical processes occurring on par (as it allows multiple frequency measurements <sup>51</sup>), diffusion-limited reactions, electron transfer rate of reaction, detection of corrosion, biosensors, or batteries studies in ion mobility and concentrations, or supercapacitors <sup>51</sup>.

In order to understand EIS results, an equivalent circuit must be matched to the data, often subjected to the interpretation of each system. In equivalent circuits, the most commonly used elements are resistors and capacitors, which depend on the associated electrochemical cell. In this work, elements such as solution resistance, charge transfer

### 2.3. Electrochemical Characterization Techniques

resistance, double layer capacitor, constant phase element, and Warburg resistance are used, being represented in the data as the Nyquist plot shown in Figure 2.6 a). In Table 2.1 the most common circuit elements are listed.

Table 2.1.: Most common circuit elements used in equivalent circuits and its impedance significance.

Element	Unit	Impedance
Resistor	$\Omega$	$Z = R$
Capacitor	F	$1/(j \omega c)$
Warburg resistance	$\Omega$	$Y_0(j\omega^n)$
Constant phase element	F	$\sigma/\omega^{1/2} - j\sigma/\omega^{1/2}$

$R_s$  is the resistance between the working electrode and the reference electrode that is commonly associated with the electrolyte.  $C_{DL}$  represents the double layer formed at the interface between the electrode and the electrolyte solution. The charges from the electrode and the ions in solution are separated in the Helmholtz-layer, acting as a capacitor. Charge transfer resistances are originated from the electronic and ionic resistance at the electrode-electrolyte interface, and the Warburg resistance ( $W$ ) is related to the resistance of ionic diffusion in the electrolyte.

EIS is an important technique as it is used to find the values of electron transfer resistance ( $R_{CT}$ ) which helps with the understanding of the diffusion process, and in the rate-determining step of the ORR, the concentration of diffusion species, the polarization resistances, the stability of the electrode, overpotentials, the Warburg, and Nernst diffusion coefficient<sup>54,55</sup>.

## 3. Methodology

### 3.1. Preparation of Composites

#### 3.1.1. Reagents and Solutions

Polyvinylidene fluoride (PVDF) pellets with molecular weight  $\sim 275 \text{ g mol}^{-1}$ , Polyvinyl alcohol (PVA) with an average molecular weight of 26,300-30,000  $\text{g mol}^{-1}$ , Dimethyl sulfoxide (DMSO) (purity 99.9%) and N,N-Dimethylacetamide (DMA) (purity 99%) were purchased from Sigma-Aldrich and used as received.

Few-layer graphene platelets with lateral sizes between 0.5-1  $\mu\text{m}$  were purchased from Elicarb from Thomas Swan & Co. Ltd.

##### **Phosphate buffer solution**

Phosphate buffer solutions (PBS) were prepared by dissolving in distilled water different quantities of  $\text{KH}_2\text{PO}_4$  and  $\text{Na}_2\text{HPO}_4$  (reagent grade  $\geq 99.0\%$ ) and then controlling with a pH-meter to achieve *pH* with values of 2, 4, 6, 7, 8, and 10. Solutions of  $\text{H}_3\text{PO}_4$  and 0.1 M NaOH were used to adequate the *pH*.

##### **Potassium ferricyanide solution**

5 mM of  $\text{K}_3\text{Fe}(\text{CN})_6$  solution was prepared by dissolving 0.4116 g of potassium ferricyanide in a PBS solution *pH* 7 until a 250 mL volume.

#### 3.1.2. Experimental Procedure

Combinations of the polymers PVDF and PVA were prepared first for analysis. Depending on the concentration required, different amount of PVDF (0.5, 1.0, and 1.7 wt%) and PVA (0.5 and 1.5 wt%) were weighted and dissolved in DMSO and DMA.

### 3.2. Electrochemical Cell Design & Electrode Modification

The mixtures were put in the ultrasound and left for 5 hours at 35 °C. The proportion of DMSO and DMA was 50/50 by weight without the polymers.

Different quantities of graphene (0.1, 0.2, and 0.4 wt%) were added depending on the required concentration and using the polymers matrix from above. After the addition of graphene, the composites were left in the ultrasound from 30 to 60 minutes at 35 °C.

## 3.2. Electrochemical Cell Design & Electrode Modification

The electrochemical setup consisted of a three-electrode system where a glassy carbon electrode was modified with different graphene/polymer composites as the working electrode, a 3.0 M Ag/AgCl electrode as the reference, and a platinum electrode as the counter electrode. The equipment used for all measurements was an Autolab PGSTAT128N, Metrohm, Netherlands low current, and noise with a fast potentiostat/galvanostat able to measure a maximum of 800 mA equipped with FRA32M impedance spectroscopy module. Experiments were run in Nova 2.1 Software. The cell design is shown in Figure 3.1.

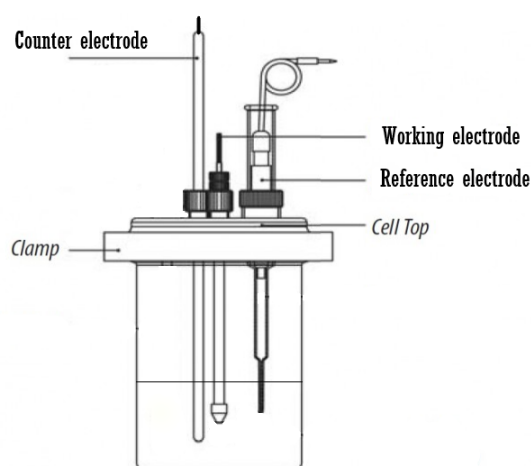


Figure 3.1.: Electrochemical cell used for all non-spectroscopic measurements.

### Glassy carbon working electrode

### 3. Methodology

The unmodified working electrode (WE) was a Glassy Carbon (GC) electrode with a 3 mm electrode diameter and Kel-F as supporting material (model CHI104, CH Instruments, USA).

#### **Silver-silver chloride reference electrode**

The electrode was a commercial Ag/AgCl reference electrode (RE) with an electrolyte concentration of 3 M KCl (6.0733.100, Metrohm, Netherlands). The working range of the electrode is 0 °C to 80 °C.

#### **Platinum counter electrode**

A platinum rod 2 mm diameter was applied as the counter electrode (CE) (0092, Metrohm, Netherlands).

#### **Electrode polishing**

As measurements depend on the quality of the sample, the electrode should be neat, meaning all the noise should be removed. In this way, by polishing the electrode, the surface is defined and becomes reactive. This process can be performed by two means, mechanical polishing and chemical polishing.

Water-alumina slurry is used for the mechanical polishing for 3 minutes and then rinsing water to remove the alumina. Chemical polishing consists of a series of CV in a 1 M H<sub>2</sub>SO<sub>4</sub> solution from an upper vertex potential of -1.5 to 1.5 V with a scan rate of 50 mV s<sup>-1</sup> for 10 cycles in order to remove any residues from the electrode surface.

#### **Electrode modification**

After the polishing and water rinsing, 7.5 μL of the chosen graphene/polymer composite were uniformly dispersed on the electrode by drop-casting and then left to dry at 40 °C for 1 hour. Finally, the electrode was allowed to cool to room temperature. The procedure is shown in Figure 3.2.

### 3.3. Electrochemical Characterization

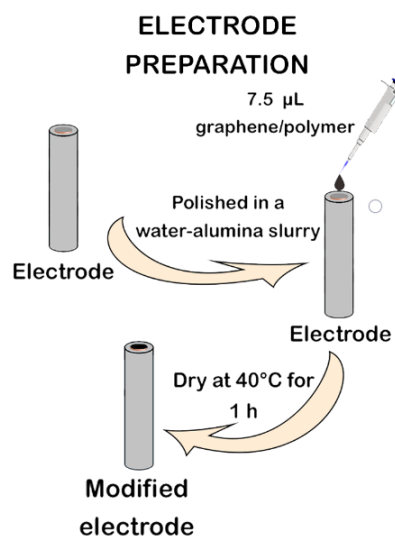


Figure 3.2.: Process to obtain a modified electrode in order to perform electrochemical measurements.

## 3.3. Electrochemical Characterization

### 3.3.1. Cyclic Voltammetry

CV was first used to obtain the thin layer optimization. Several composites were tested in order to obtain the best outcomes in terms of more current generated and low peak potential separation, as well as the relation between the cathodic and anodic peak current vs the amount of graphene in the composite. Approximately 20 mL of a ferricyanide solution in PBS at  $pH$  7, which was for 5 minutes under a nitrogen atmosphere, was used.

CV technique was also used to obtain information about the current generated in the ORR and its dependence with the amount of graphene, the interaction of the catalyst with the electrolyte or the catalytic activity of the catalysts, values of the onset potentials and its dependence with the amount of graphene and the variation of  $pH$ , and overpotentials. In this case, approximately 20 mL of a phosphate buffer solution with values of  $pH$  of 2, 4, 6, 8, and 10 was used. The solution was purged with air for 5

### 3. Methodology

minutes for each measurement.

#### 3.3.2. Electrochemical Impedance Spectroscopy

A 5mM ferricyanide solution in PBS (around 20 mL) purged with nitrogen for 5 minutes to remove dissolved oxygen was used. Measurements were performed from 0.01 to 10,000 Hz. If necessary, a high-frequency shunt was used to remove artifacts. All EIS measurements were performed using a Faraday cage to reduce noise<sup>56</sup>, as shown in Fig 3.3.

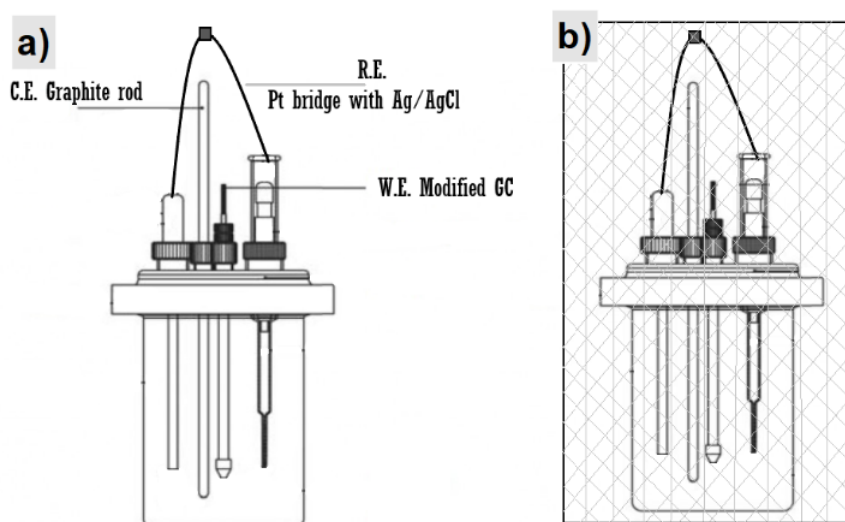


Figure 3.3.: a) Electrochemical cell and electrodes used for EIS measurements. b) Overall setup using a prototype of a Faraday cage for EIS measurements.

EIS was performed to analyze the correlation between the amount of graphene in the composite and changes in the charge transfer resistance  $R_{CT}$ , which indicates electrocatalytic activity.

## 4. Results and Discussion

### 4.1. Spectroscopic Characterization

Spectroscopic characterization was conducted by Raman spectroscopy in order to determine the composition of the composites. Graphene has been extensively studied since its discovery as it is a carbon allotrope with different possible applications, and the Raman spectrum of the composite is widely known.

The composites of interest were formed by a polymeric matrix of PVDF and PVA and then an addition of graphene. Fig. 4.1 b) shows the PVDF spectrum in a 500-2000  $\text{cm}^{-1}$  range. It shows a peak around 800  $\text{cm}^{-1}$ , which can be used to reveal that PVDF is in alpha phase<sup>57</sup>. Studies show that the  $\alpha$ -PVDF activation peak is at 794  $\text{cm}^{-1}$ <sup>58</sup>, and it is formed by  $(\text{CH}_2\text{-CF}_2)_n$  chains in a monoclinic crystalline system; and it can be differentiated from the beta phase, because of the absence of its characteristic peak shift towards 840  $\text{cm}^{-1}$ . The peak found at 1433  $\text{cm}^{-1}$  corresponds to the CH stretching vibrational mode<sup>59</sup>.

PVA Raman spectrum has typically vibrational modes attributed to the  $\text{CH}_2\text{-CHOH-}$  moiety with peaks at 1432  $\text{cm}^{-1}$  for a  $\text{CH}_2$  bending, 1362  $\text{cm}^{-1}$  for  $\text{CH}_2$  wagging and rocking modes, 1096  $\text{cm}^{-1}$  for the vibrational CO band, 922  $\text{cm}^{-1}$  skeletal C-C vibration and an attributed CH and OH vibrational mode at 1440  $\text{cm}^{-1}$ <sup>60</sup>. Fig. 4.1 a) shows the PVA spectrum in a 500-2000  $\text{cm}^{-1}$  range, where the 1096, the 1440, and the 922  $\text{cm}^{-1}$  peaks are found, and the main 880  $\text{cm}^{-1}$  peak is associated with the stretching of C-COO.

The graphene powder (in Figure 4.1 c)) shows the so-called defect or D-band around 1350  $\text{cm}^{-1}$ , which is inactive because of a zone boundary mode and can be activated

#### 4. Results and Discussion

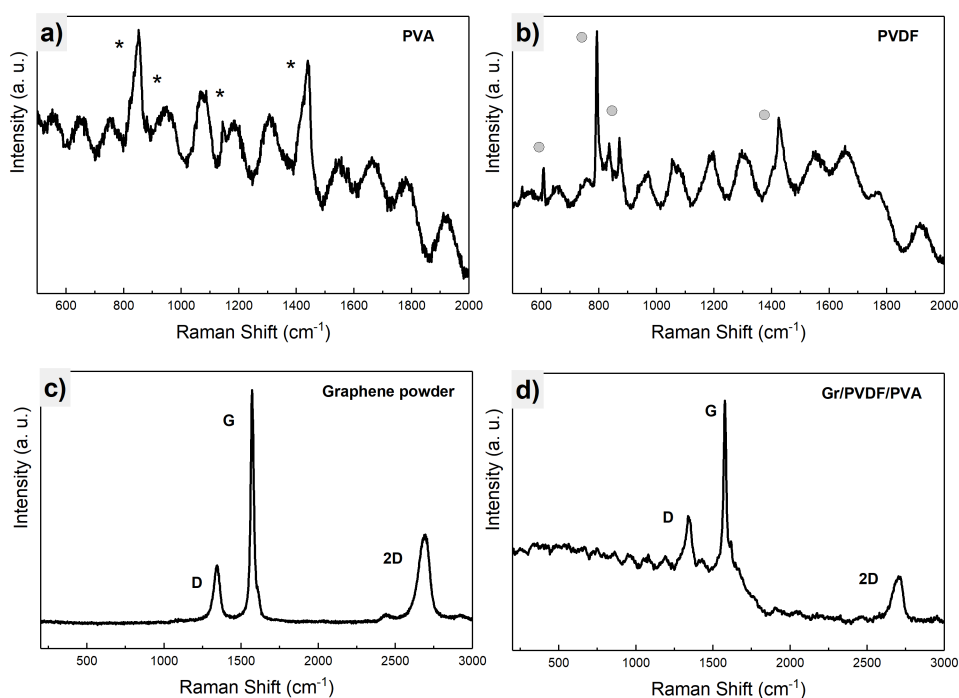


Figure 4.1.: Typical Raman spectra excited with an Nd: YAG laser ( $\lambda = 532$  nm) of a) PVA and b) PVDF polymers precursors, c) few layers graphene nanoplatelets powder and d) Gr/PVDF/PVA nanocomposites consisting of 0.5 wt% PVDF/PVA and 0.2 wt% Graphene. D, G, and 2D bands and the relevant bands of PVA (stars) and PVDF (closed circles) are marked.

by a double-resonance phenomenon. Another band is the strong G-band around  $1580\text{ cm}^{-1}$ , corresponding to carbon-carbon in-plane stretching in graphitic materials. And also, a vibrational band at  $2700\text{ cm}^{-1}$  characteristic for graphene compounds, known as a second-order vibrational mode of the D band, named the 2D band<sup>61</sup>. As the type of graphene used was few layers graphene, it is important to mention that the G-band increases when increasing the layers of graphene<sup>61</sup>.

The final Figure 4.1 d) shows the spectrum for a composite of 0.2% Graphene / 0.5% PVDF / 0.5% PVA and can easily prove the presence of graphene, with the D, G, and 2D bands. The polymeric matrix is associated with the noise-type of background with an increased intensity that does not appear in c). This effect is a typical background corresponding to the photoluminescence of the polymeric matrix, because of the vibra-

tional modes in the compounds.

## 4.2. Thin Layer Optimization

### 4.2.1. Cyclic Voltammetry

#### Pristine polymers

As graphene is hydrophobic, the need for an adequate solvent used to disperse and create a stable suspension is mandatory. PVDF is a non-reactive and easy to use material, that can dissolve in common organic solvents and is thermodynamically compatible, meaning that is able to mix with other polymers<sup>62</sup>. Yang and collaborators<sup>63</sup> used an activated carbon with PVDF as a binder composite as cathode for an MFC, varying the concentration of PVDF from five to ten percent weight, in the overall composite. The polymeric concentration and ratio in the overall composite are important variables because a good adhesion between the components and the additives is necessary for graphene to be well dispersed in the polymeric matrix.

Ferricyanide is a commonly used redox probe because of its highly redox reversible character and single electron transfer reaction from ferricyanide  $[\text{Fe}(\text{CN})_6]^{3-}$  to ferrocyanide  $[\text{Fe}(\text{CN})_6]^{4-}$ . Polyvinyl alcohol (PVA) is a polymer that can increase the electrical conductivity of a composite when added to a nanocarbon compound<sup>64</sup>. The mixture of PVDF and PVA has been studied to use them as membranes to separate arsenic or dyes from aqueous solutions<sup>65,66</sup>, looking for improvements in hydrophilicity, permeability, and mechanical properties.

Figure 4.2 shows the CV response to the mentioned systems. PVDF (red curve) shows a current extremely low compared to the other composites, as this is a non-conductive and electrochemically stable polymer, inhibiting the redox reaction of ferricyanide. On the other side, PVA (blue curve) shows a clear increase in current at 0.13 V

#### 4. Results and Discussion

and 0.32 V vs. Ag/AgCl, with a cathodic peak current of  $\sim -20 \mu\text{A}$ . This response from PVA is because it is a more conductive compound than PVDF, with hydroxyl groups on its structure, which facilitate interactions with itself and other compounds.

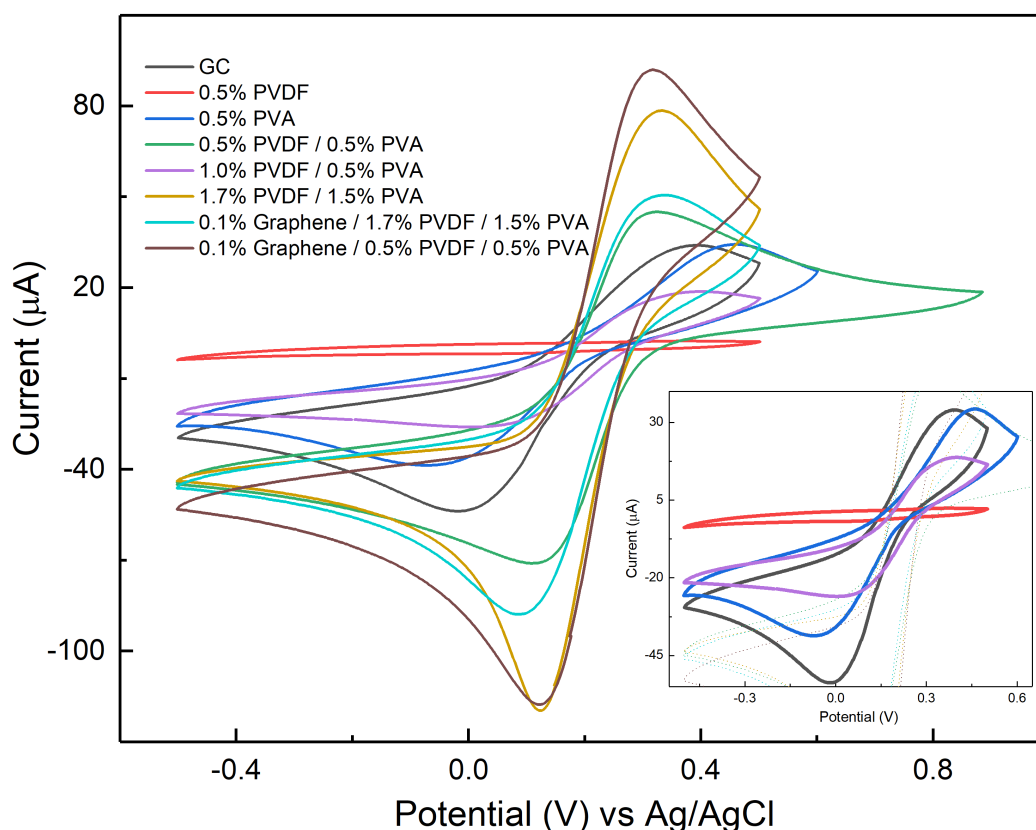


Figure 4.2.: Cyclic voltammograms for the different types of polymers, polymeric mixtures, first graphene composites, and the GC reference. Inset: magnification of the systems with the lowest currents. Measurements were performed in a nitrogen saturated 5mM ferricyanide solution in PBS, against Ag/AgCl reference electrode, at a scan rate of  $0.1 \text{ V s}^{-1}$ , at  $25^\circ\text{C}$ .

#### Polymeric matrixes

The first results showed that in composites formed just by PVDF and graphene, no reduction nor oxidation processes were seen in the cyclic voltammograms, so PVA was added to the matrix. This mentioned mixture of polymers was used for the composites, as PVDF by itself did not provide an adequate environment for a redox reaction to

## 4.2. Thin Layer Optimization

occur due to its highly electrically resistive nature.

After the best polymeric matrix was determined to be a mixture of PVDF and PVA, alternations in their concentrations in the matrix were studied. In the same Fig. 4.2 the voltammograms of the 0.5% PVDF / 0.5% PVA, 1.0% PVDF / 0.5% PVA and 1.7% PVDF / 1.5% PVA composites are shown, with a similar pattern in the cathodic and anodic potentials as that from PVA. Yet, the difference comes when analyzing the current generated and the peak potential separation of the composites<sup>67</sup>, being the last composition mentioned the one with the highest peak current of  $\sim -100 \mu\text{A}$  and the lowest  $\Delta E_p$  of 0.208 V.

It is important to mention that a 0.5% PVDF / 1.5% PVA composite was also studied, yet the composite showed a bad adhesion to the electrode when performing the CV. A possible explanation for the behavior of the polymers is that at high contents of PVDF in the matrix (as shown in the purple curve in Fig. 4.2), the conductivity of the composite decreases, being the lowest from the three studied compositions. On the other hand, if high amounts of PVA in relation to PVDF are added to the matrix, the polymers will aggregate, forming a nonuniform layer in which the electron exchange between the electrode and the solution is not possible, not allowing any measurements.

When the same composition is set for both polymers, the results are better, with an increase in the current and a decrease in  $\Delta E_p$  as a function of the amount of polymer added (as can be seen for green and an even better yellow curves in Fig. 4.2). It is important to take into account the little quantity of polymers used as compared to the literature, where amounts of up to 10 wt% are used<sup>63</sup>.

### **Graphene-polymeric matrix composites**

Subsequently, the addition of graphene to the polymeric mixture was studied, starting with the addition of 0.1 wt% of graphene to the 1.7% PVDF / 1.5% PVA and to the 0.5% PVDF / 0.5% PVA matrixes. It is to be expected that the current will increase with the

#### 4. Results and Discussion

addition of graphene given its high conductivity, yet the first composite mentioned, decreased its cathodic peak current from  $-100 \mu\text{A}$  to  $-70 \mu\text{A}$  (as shown in yellow and sky blue curves in Fig. 4.2). This effect can be caused because of agglomeration of the graphene particles, not allowing a correct current path for electrons to flow and hence, decreasing the current generated. The ratio graphene/polymer should be controlled in order for graphene to provide its conductivity properties to the overall composite<sup>62</sup>.

On the other hand, the second composite mentioned showed the expected improvements, as the addition of graphene increased the cathodic peak current from  $-65 \mu\text{A}$  to  $-112 \mu\text{A}$  and decreased the  $\Delta E_p$  from  $0.21 \text{ V}$  to  $0.19 \text{ V}$  (as represented by the green and brown curves in Fig. 4.2). Given these results, the 0.5% PVDF / 0.5% PVA was chosen as the polymeric matrix for all remaining graphene composites.

Further analyses were performed by increasing the quantity of graphene in the polymeric matrix, which is represented in the voltammograms shown in Fig. 4.3 a). Results show a great difference in current between the matrix without graphene, and the composite with a 0.1 wt% addition for both cathodic and anodic peak currents. The 0.4 wt% composite shows the highest cathodic peak with  $-132.7 \mu\text{A}$  and the lowest  $\Delta E_p$  of  $0.171 \text{ V}$  vs. Ag/AgCl responding to the understandable tendency for current to increase as graphene content is increased, because of its high conductivity and increased charge transfer kinetics of the electrode.

Figure 4.3 b) shows the cathodic peak current and d) the anodic peak current relation with the graphene content of composites. In b) the peak current initially increases rapidly until it seems to stall at 0.2 up to 0.4 wt%, as shown in the red curve. In d), a similar path is observed. All graphene composites showed better performance than the polymeric matrix. The explanation for this behavior is that graphene particles provide the major part of the electrical conductivity to the composite, as well as faster electron transfer which provides a greater current, and faster reaction kinetics which ends in lower values of  $\Delta E_p$ . PVA has hydroxyl groups that can be cross-linked with

## 4.2. Thin Layer Optimization

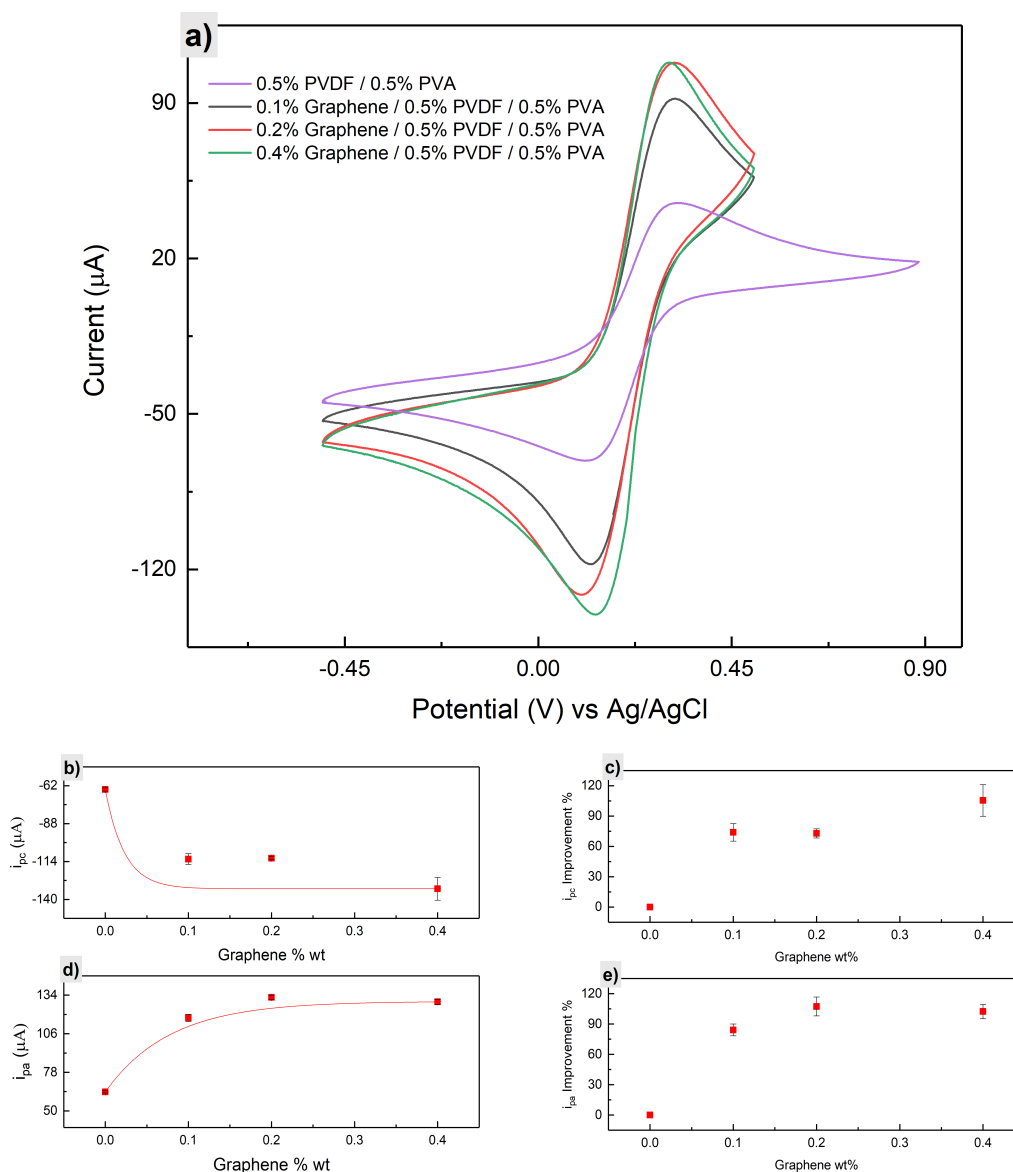


Figure 4.3.: a) Cyclic voltammograms for the the 0.5% PVDF / 0.5% PVA mixture and graphene composites. Measurements were performed in a nitrogen saturated 5mM ferricyanide solution in PBS, against Ag/AgCl reference electrode, at a scan rate of  $0.1 \text{ V s}^{-1}$ , at  $25 \text{ }^\circ\text{C}$ . And a representation of b) cathodic and d) anodic peak currents vs the graphene mass percentage composition and its improvements in c) and e).

the functional groups of graphene and form a conductive composite <sup>62</sup>; this means that electrons can move easier from the electrode to the composite and to the  $\text{Fe}^{3+}$  and reduce it to  $\text{Fe}^{2+}$ . This improves the current generated as the compound has better facility to allow more electrons to be transferred.

Table 4.1 shows the cathodic and anodic peak current values, as well as the peak

#### 4. Results and Discussion

Table 4.1.: Cathodic and anodic peak currents, and peak potential separation of the different composites.

Composites			$i_{pc}$ ( $\mu A$ )		$i_{pa}$ ( $\mu A$ )		$\Delta E_p$ (mV)	
% PVDF	% PVA	% Gr.	Value	Error %	Value	Error %	Value	Error %
0.5	0.5	–	-64.6	$\pm 1.1$	63.8	$\pm 0.8$	214.8	$\pm 0.8$
0.5	0.5	0.1	-112.3	$\pm 3.7$	117.5	$\pm 2.6$	197.8	$\pm 2.2$
0.5	0.5	0.2	-111.7	$\pm 1.0$	132.3	$\pm 1.6$	217.3	$\pm 4.3$
0.5	0.5	0.4	-132.7	$\pm 7.8$	129.1	$\pm 1.9$	170.9	$\pm 2.9$
–	0.5	–	-19.8	$\pm 2.4$	30.1	$\pm 0.5$	529.8	$\pm 0.8$
1.0	0.5	–	-10.5	$\pm 0.07$	23.4	$\pm 0.3$	395.5	$\pm 1.6$
1.7	1.5	–	-99.9	$\pm 1.0$	104.4	$\pm 1.3$	207.5	$\pm 1.6$
1.7	1.5	0.1	-70.4	$\pm 3.9$	73.6	$\pm 0.7$	253.9	$\pm 6.5$

potential separation of the composites studied. From the recovered information, there is an improvement of 325% from the cathodic peak current of PVA to that of the chosen polymeric matrix PVDF/PVA and 212% for the anodic peak current. Now, as shown in Figure 4.3 c), from the matrix, there is an increase of 74% to the first addition of graphene, and a 105% to the 0.4% for  $i_{pc}$  and an increase of 84% and 102% respectively for the  $i_{pa}$  (as shown in Fig. 4.3 e)).

The best performance was obtained by the 0.4 wt% graphene content composition, yet when comparing cost-benefit performance, the 0.2 wt% composite proves to be better, as there is an overall small difference in the improvement, with 0.2 wt% of graphene less. Table 4.2 summarizes all the composites studied in the ferricyanide solution and discussed in this section. In the next section, further information about these same composites to complement the analysis about the possible catalysts to probe the catalytic activity will be performed by EIS measurements.

## 4.2. Thin Layer Optimization

Table 4.2.: Polymer and graphene compositions of the different types of composites prepared to be studied as electrodes.

PVDF (wt%)	PVA (wt%)	Graphene (wt%)	Observations
0.5	–	–	No current peaks/Good Adhesion
–	0.5	–	Visible Current peaks/Good Adhesion
0.5	0.5	–	High current peaks/Good Adhesion
0.5	0.5	0.1	High current peaks/Good Adhesion
0.5	0.5	0.2	High current peaks/Good Adhesion
0.5	0.5	0.4	Highest current peaks/Good Adhesion
1.0	0.5	–	Lowest current peaks/Good Adhesion
0.5	1.5	–	Bad adhesion
1.7	1.5	–	Highest current peaks for polymers
1.7	1.5	0.1	Adding graphene decreased current peaks

### 4.2.2. Electrochemical Impedance Spectroscopy

The importance of studying the electrode's impedance is to be able to interpret the behavior of the coating and to know more about the electrode-electrolyte interface. The charge transfer resistance ( $R_{CT}$ ) shows the ease of the electron transfer from the electrode to the redox species in solution. According to the previous CV results shown in Section 4.2.1., the electrodes containing higher graphene composition are expected to show the lowest value of ( $R_{CT}$ ) as they showed the highest peak currents generated.

In Fig. 4.4 the Nyquist plots for the different composites are shown. Preliminary results show the highest impedances for the polymers without graphene addition (red and blue curves), together with the composites with the lowest graphene concentrations (purple and dark yellow curves), while the higher graphene concentration of 0.4 wt% composite showed the lowest impedance. These results of each electrode and the used equivalent circuits will be discussed below in more detail.

#### 4. Results and Discussion

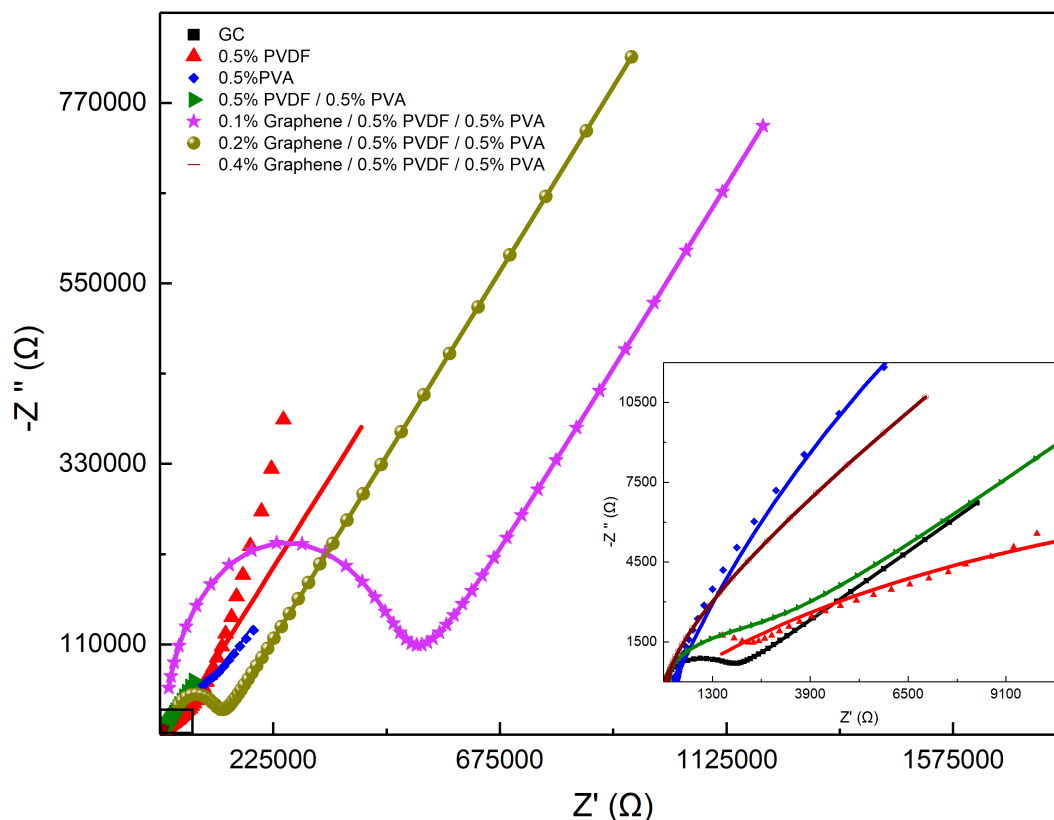


Figure 4.4.: Nyquist plot for all composites in a 5mM ferricyanide in PBS solution at OCP and 25 °C. Inset: Magnification of the impedance at higher frequencies. Symbols: Experimental data. Continuous lines: Fit.

#### Glassy carbon electrode

The glassy carbon electrode is the support on top of which the drop-casting was performed for all composites. By performing EIS for this electrode, to some extent, the electrolyte resistance can be estimated for this solution and setup. In order to understand the data, an equivalent circuit must be associated with the system. In this case, a Randles circuit (shown in Fig. 4.5) can easily do the job, with an electrolyte resistance correspondent to that of the ferricyanide in PBS solution, a double layer capacitance which is formed at the interface electrode/electrolyte, a charge transfer resistance, and a Warburg resistance correspondent to the diffusion contributions. Nyquist plot for

## 4.2. Thin Layer Optimization

this electrode is already shown in Fig. 4.4 as the black curve, and it shows that at high frequencies, a semicircle is obtained as a representation of the charge transfer resistance, and then at lower frequencies, a straight line shows the diffusion contribution.

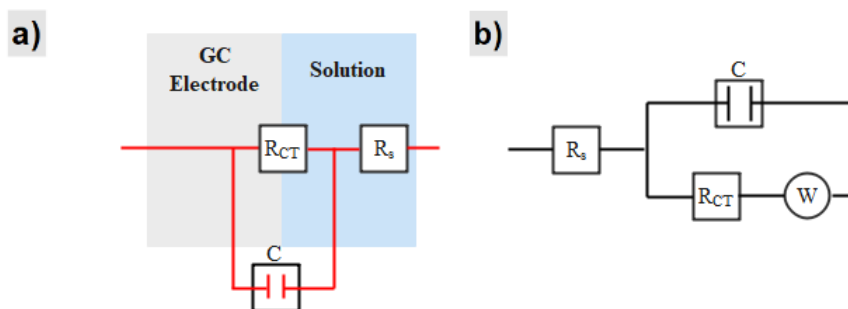


Figure 4.5.: a) Schematic representation of the cell and the electric elements present on it, and b) Randles equivalent circuit for the fitting of the GC data.

The Randles circuit was a good fit for the data, and the results obtained with it are shown in Table 4.3 with an  $R_s$  of 86.8  $\Omega$  that should be similar for the other composites, as  $R_s$  is only related to the electrolyte and the cell dimensions. The charge transfer resistance has a value of 1,567  $\Omega$ , which shows an easy transfer of the electrons from the electrode to the solution specie. The major part of the impedance comes from diffusion contributions, and the composite shows a really low capacitance of 1.3  $\mu\text{F}$  due to a relatively low surface area of glassy carbon.

Table 4.3.: Equivalent circuit parameters for GC

	Value	Error %
$R_s$ ( $\Omega$ )	86.8	< 0.1
$R_{CT}$ ( $\Omega$ )	1567	< 0.1
C (F)	1.3 E <sup>-6</sup>	< 0.1
W ( $\Omega$ )	3357.7	< 0.1

#### 4. Results and Discussion

##### Polymers

EIS results for polymers should follow the trend outlined in the CV experiments, PVDF being a bad conductor showing high impedance, PVA with a slight improvement compared with the other polymer, but also with high impedance values and a clear improvement for the mixture of these two composites with the lowest impedance value for the three. In this case, a modified Randles circuit (shown in Fig. 4.6) is associated with the two polymers, with a constant phase element (CPE) instead of a  $C$  as the capacitor. A CPE confirms a frequency dispersion originated from some kind of surface disorder, or inhomogeneity at the electrode surface<sup>68</sup>, which fits the case as the polymer creates an agglomeration in the electrode surface, making it a good fit. The common Randles circuit shown in Figure 4.5 was fitted to the mixture of polymers.

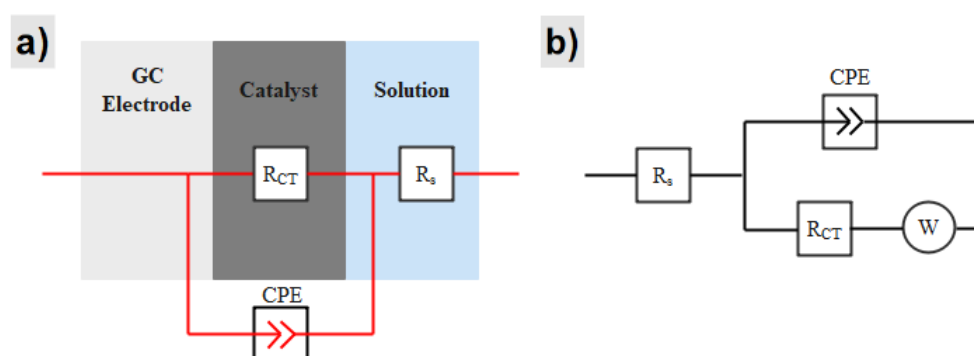


Figure 4.6.: a) Schematic representation of the cell and the electric elements present on it, and b) modified Randles circuit for the fitting of the Nyquist plot for the different polymeric composites.

Fig. 4.7 a) shows the Nyquist plot for the three compounds, where the two polymers by themselves show a not perfect fitting to the circuit with high errors, and values for  $n$  of 0.5 for PVDF and 0.8 for PVA. This value is related to the frequency dispersion and ranges between 0 and 1, with the CPE behaving as a resistor when the value is zero, and as a capacitor if the value is 1. The low  $n = 0.5$  value of PVDF indicates a very rough surface, while  $n = 0.8$  for PVA indicates a more homogeneous surface morphology.

The Warburg resistances for both polymers show really high values because of the

## 4.2. Thin Layer Optimization

diffusion contributions from the system.  $R_{CT}$  values are 26,745 and 79,409  $\Omega$  for PVDF and PVA, respectively, which show that in PVDF, the electron transfer is faster than in PVA, while  $CPE$  values of both compounds are rather low, with PVA showing a better capacitive behavior because of a higher porosity of this polymeric membrane.

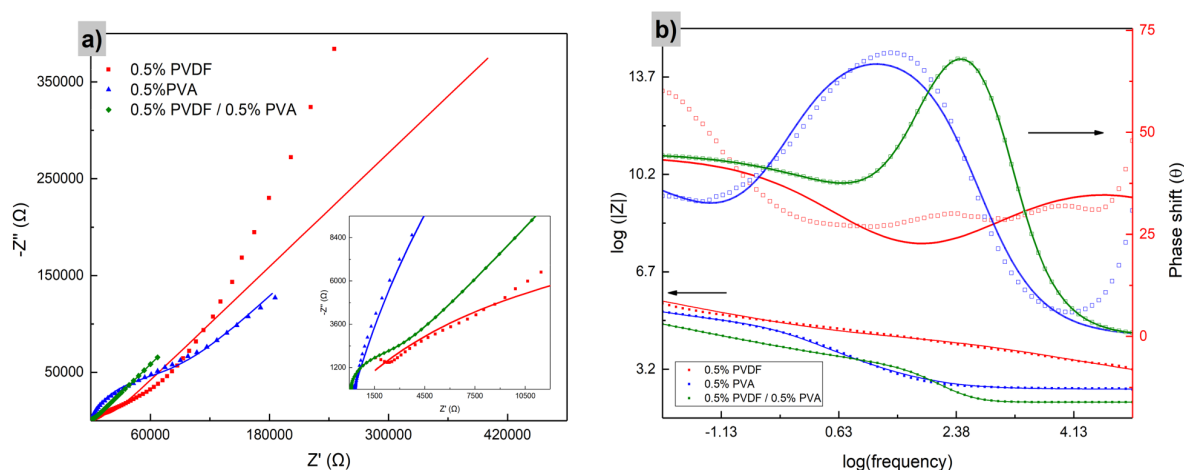


Figure 4.7.: Representation of a) Nyquist and b) Bode plots for the different polymer composites. Inset: Magnification of the systems with lower impedance. Symbols: Experimental data. Continuous lines: Fit.

On the other hand, the mixture of both polymers showed better results than the polymers themselves using a Randles circuit, with a good fitting, small errors and a solution resistance close to that of glassy carbon. The capacitance of the mixture presents the lowest value of the three with 1.0  $\mu\text{F}$ , which means that this composite has the lowest ability to collect and store energy in the form of electrical charge, caused by the correct mixing of both polymers, in which PVDF causes a decrease in the porosity that PVA showed previously.

There is a semicircle at high frequencies corresponding to the charge transfer resistance, which is 36 times lower than that of PVA and 12 times lower than PVDF, which shows the improvement regarding the ease of the electron transfer, demonstrating the good response of mixing both polymers.

In Figure 4.7 b, the bode plot for all the mentioned polymeric compounds is shown,

#### 4. Results and Discussion

where the lower impedance of the polymeric mixture is better noticed as the green curve and PVDF (red curve) has the higher impedance. This behavior is explained by the low conductivity of PVDF, not allowing electrons to easily flow towards the electron acceptor specie. The addition of PVA enhances this property, allowing electrons to flow and decreasing the  $R_{CT}$  value. PVA shows a slight deviation from the fitting with a phase angle of  $68^\circ$  that is also corroborated in the polymeric mixture with the same angle but at different frequencies (blue curves). All these results for the three polymers are shown in Table 4.4.

Table 4.4.: Equivalent circuit parameters for the polymer composites

	0.5% PVDF		0.5% PVA		0.5% PVDF / 0.5% PVA	
	Value	Error %	Value	Error %	Value	Error %
$R_s$ ( $\Omega$ )	249.7	$\pm 89.1$	306.3	$\pm 7.4$	104.1	$< 0.1$
$R_{CT}$ ( $\Omega$ )	26745	$\pm 16.3$	79409	$\pm 12.0$	2211.7	$< 0.1$
CPE / C (F)	$1.2 E^{-6}$	$\pm 6.4$	$4.6 E^{-6}$	$\pm 5.3$	$1.0 E^{-6}$	$< 0.1$
W ( $\Omega$ )	133730	$\pm 16.1$	32725	$\pm 16.1$	16407	$< 0.1$
n	0.5	$\pm 3.0$	0.8	$\pm 1.7$	–	–

#### Graphene addition

The information retrieved from the addition of graphene is quite different from the previous result, as the 0.1 and 0.2% graphene compositions have impedance values even higher than those of the polymers. In this case, there were two different equivalent circuits used. The two first graphene composites were fitted by a Randles equivalent circuit (as Fig. 4.5), then the 0.4% composite was fitted by the circuit shown in Fig. 4.8, whose circuit models a cell where polarization is due to a combination of kinetic and diffusion processes<sup>51</sup>.

In Fig. 4.9 a the Nyquist plot for the graphene composites shows that when graphene

## 4.2. Thin Layer Optimization

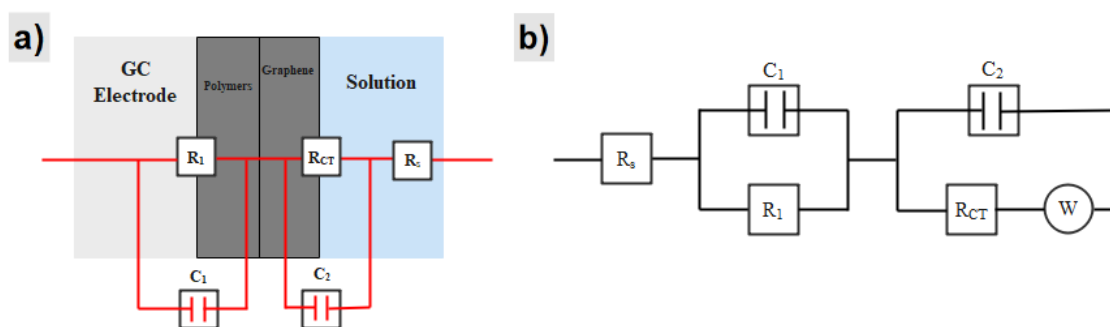


Figure 4.8.: a) Schematic representation of the cell and the electric elements present on it, and b) modified two-part circuit for the fitting of the Nyquist plot for the different graphene/polymer composites.

is added, the  $R_{CT}$  values decrease. This behavior is expected as graphene increases the conductivity of the system, decreasing the charge transfer resistance. Table 4.5 shows the result of the fits for the graphene composites. It shows that the first and second composite demonstrate a good fitting with small errors, and that the last composition has an increase in the error percentage.

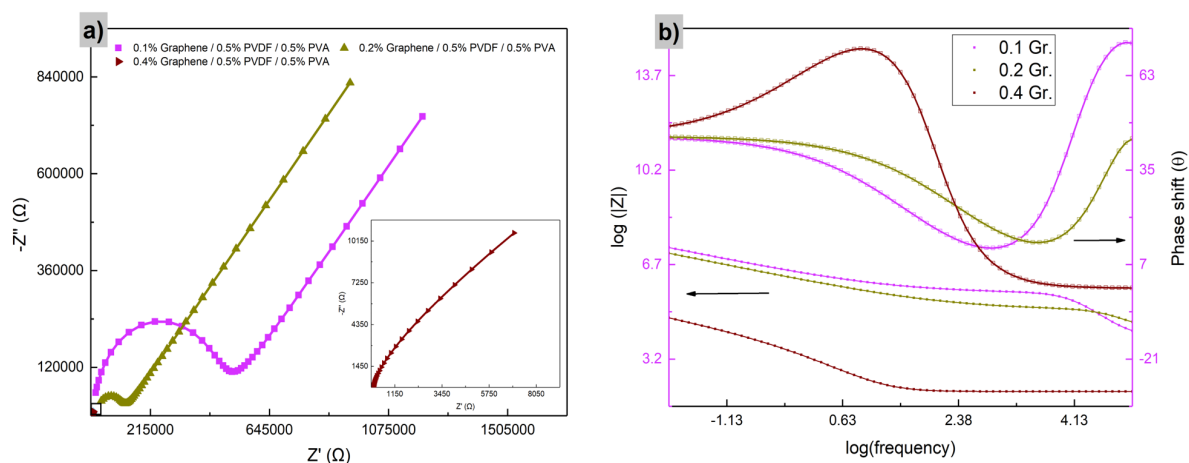


Figure 4.9.: Representation of a) Nyquist and b) Bode plots for the different graphene/polymer composites. Inset: Magnification of the systems with lower impedance. Symbols: Experimental data. Continuous lines: Fit.

The capacitance is the highest for the 0.4 wt% composite with  $15.5 \mu F$ , with an explanation in the porosity of graphene where oxygen is adsorbed; as the amount of graphene increases, the porosity increases and hence the capacitance increases. The

#### 4. Results and Discussion

different values of charge transfer resistance can be observed in Fig. 4.10 a) where the 0.4 wt% also shows a value 4.7 times lower than that for the polymeric matrix, which is the expected behavior when adding graphene to the composite.

Table 4.5.: Equivalent circuit parameters for the graphene/polymer composites

	0.1% Gr. / 0.5% PVDF / 0.5% PVA		0.2% Gr. / 0.5% PVDF / 0.5% PVA		0.4% Gr. / 0.5% PVDF / 0.5% PVA	
	Value	Error %	Value	Error %	Value	Error %
$R_s$ ( $\Omega$ )	10606	< 0.1	20474	< 0.1	99.7	< 0.1
$R_1$ ( $\Omega$ )	–	–	–	–	3.0	$\pm 11.4$
$R_{CT}$ ( $\Omega$ )	448600	< 0.1	91115	< 0.1	468.5	$\pm 1.2$
$C_1$ (F)	$2.7 E^{-11}$	< 0.1	$3.5 E^{-11}$	< 0.1	$5.0 E^{-4}$	$\pm 26.7$
$C_2$ (F)	–	–	–	–	$1.6 E^{-5}$	$\pm 0.1$
$W$ ( $\Omega$ )	5233600	< 0.1	3280300	< 0.1	14772	$\pm 0.1$

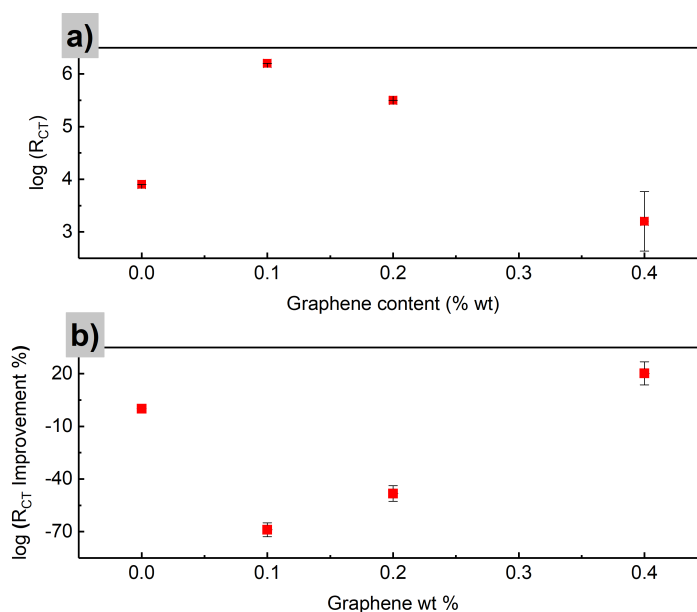


Figure 4.10.: a) Charge transfer resistance as a function of the amount of graphene in the composite and b) its improvement.

For the Bode plot shown in Fig. 4.9 c) different phase angles can be obtained for the

### 4.3. Catalytic Activity towards ORR

four different composites, and a clearer tendency of how the impedance changes with the composites, where the 0.4% composite has the lowest value. Figure 4.10 b) shows the improvement that the graphene composites have in terms of  $R_{CT}$ , where the explanation given above can be better understood. The two first graphene compositions do not show improvements over the polymeric matrix as their values of  $R_{CT}$  increases, then the 0.4 wt% composite resulted in the lowest value of charge transfer resistance and an improvement of 20.1%, showing the best results.

### 4.3. Catalytic Activity towards ORR

The catalytic activity of the composites was studied by cyclic voltammetry in an air-saturated PBS solution at different  $pH$ . As shown by the previous experiments detailed in Section 4.2., the pure PVDF, PVA, the 1.0% PVDF / 0.5% PVA, and the 0.1% Gr. / 1.7% PVDF / 1.5% PVA samples showed very low current peaks as well as high impedances, which labels them as unpromising candidates, so their catalytic activities were therefore not studied here.

The  $pH$  of the medium is studied because of the possible application the coated electrode could have in the different fields in which oxygen reduction reaction is needed. For example, in microbial fuel cells, the  $pH$  must be basic in order for bacteria to live and develop, so a basic  $pH$  should be required. Basic  $pH$  are often associated with easier to reach electrocatalytic performances than acidic mediums because of its lower standard reduction potential (0.401 V vs. NHE at  $pH = 14$ ) required to reduce oxygen

16.  
Fig. 4.11 shows all the voltammograms studied and their behavior within a potential range of -0.6 V to -0.005 V, starting at the open cell potential at different  $pH$ . As it can be observed, all composites show the highest cathodic current at acidic  $pH$ s ( $pH = 2$  or 4 shown as black and red curves). As graphene content increases, it is expected that the

#### 4. Results and Discussion

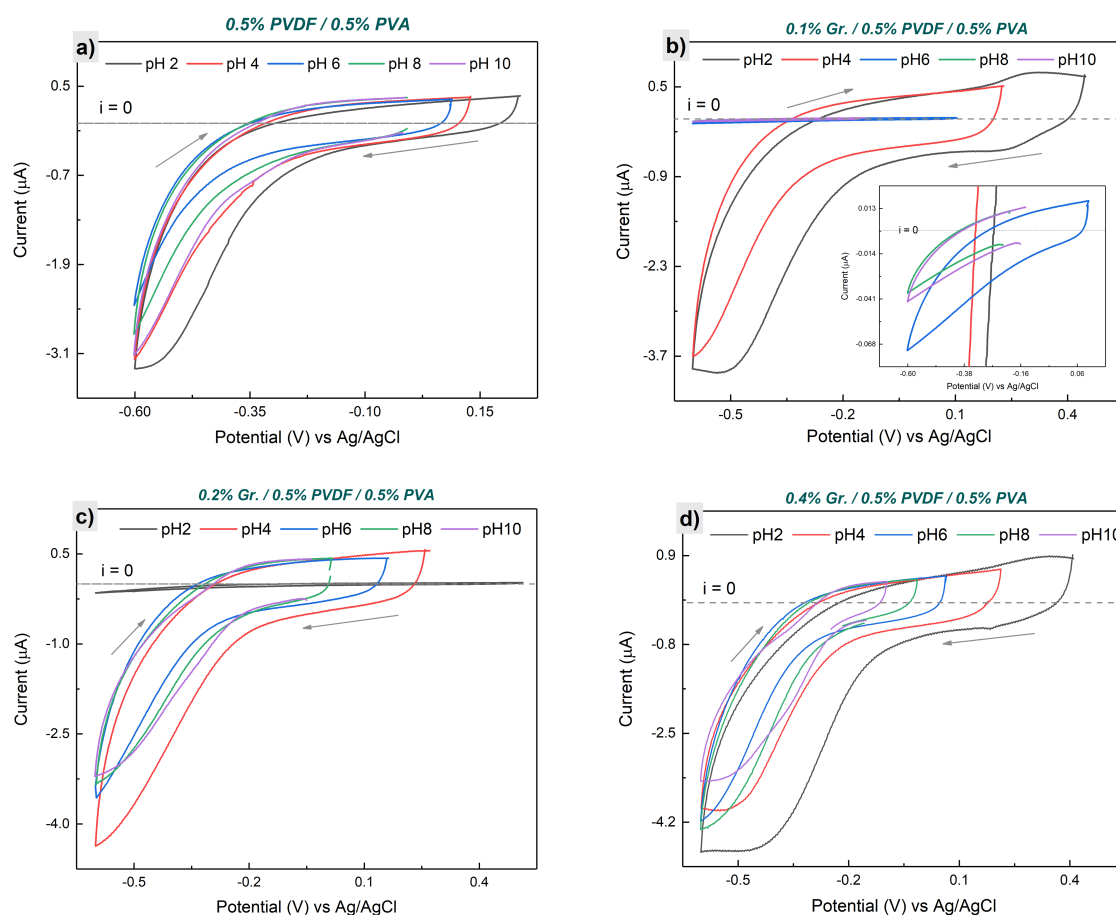


Figure 4.11.: Cyclic voltammetry of all composite electrodes for the study of catalytic performance. The scans were recorded at different  $pH$  in air-saturated PBS solution at a scan rate of 10 mV/s against Ag/AgCl at 25 °C. The arrows indicate the scan direction starting at the OCP. Inset: magnification of the systems with lower catalytic activity.

electrode shows increased performance at every  $pH$  because of the high conductivity that graphene provides. The composite with 0.4 wt% graphene added in the polymeric matrix is the composite with the highest cathodic peak from all with a current of 4.8  $\mu A$  at -0.6 V vs. Ag/AgCl and at  $pH = 2$ . It is also the only composite, besides the polymeric mixture, with a leveled current generated at every  $pH$ , fact that cannot be observed for the values of the other graphene compositions.

From the voltammograms in Fig. 4.11, the approximate value of the onset potential can be obtained. This is a key factor that gives information about the catalytic capacity of the electrode. It allows to evaluate the minimum potential needed to start the re-

### 4.3. Catalytic Activity towards ORR

action; the more positive the value, the better the catalytic activity<sup>69</sup> as the reaction is studied to reduce oxygen. Table 4.6 contains the current generated by each composite at different *pH*s.

Table 4.6.: Cathodic current generated at each composite at -0.6 V vs. Ag/AgCl at different *pH*s.

<i>pH</i>	<b>Current (<math>\mu\text{A}</math>) <math>\pm</math> 0.1</b>			
	<b>0.5% PVDF / 0.5% PVA</b>	<b>0.1% Gr. / 0.5% PVDF / 0.5% PVA</b>	<b>0.2% Gr. / 0.5% PVDF / 0.5% PVA</b>	<b>0.4% Gr. / 0.5% PVDF / 0.5% PVA</b>
2	-3.3	-3.9	-0.2	-4.8
4	-3.2	-3.7	-4.3	-4.0
6	-2.5	-0.7	-3.5	-4.2
8	-2.8	0.0	-3.3	-4.3
10	-3.1	0.0	-3.2	-3.4

The dependence of the catalytic activity on the *pH* is mainly because of the quantity of ions,  $\text{H}^+$  or  $\text{OH}^-$ , present in the solution as a factor to the rate-determining step of the reaction, which is related to the number of electrons exchanged. In the case of ORR, reactions [1] and [4] show an oxygen reduction via a four-electron pathway, where  $\text{H}^+$  is part of the reaction, whereas in reactions [2] and [5]), the reduction is via a two-electron path where  $\text{OH}^-$  are released from the system.

Figure 4.12 a) shows the onset potential as a function of *pH* and figure 4.12 b) as a function of the graphene content. The polymeric matrix (in black squares) presents the more negative values for onset potential as it is expected, when graphene is added, the values go towards positive potentials in all the different *pH*, showing an improved catalytic activity for these composites.

Figure 4.12 a) also shows that the tendency of the onset potential when *pH* increases is for it to go towards more negative values. This can be explained by looking at the

#### 4. Results and Discussion

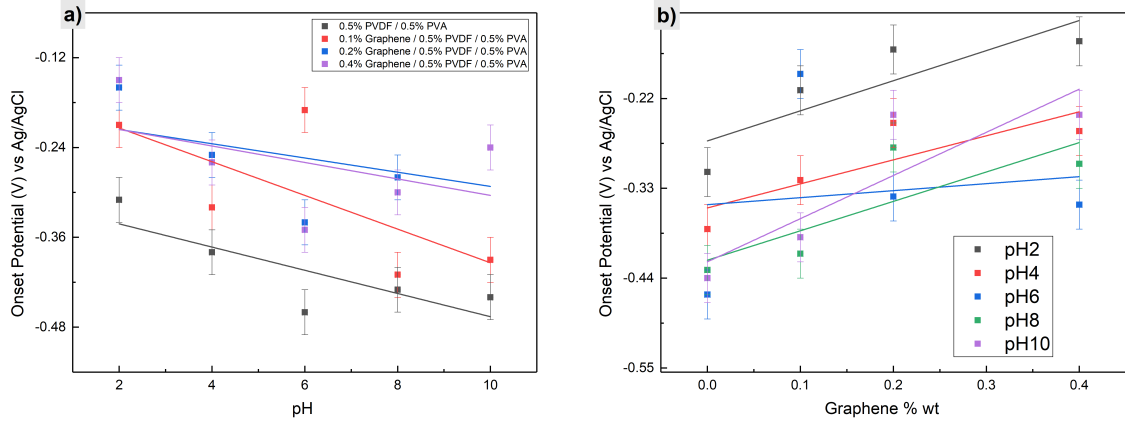


Figure 4.12.: Onset potential (vs. Ag/AgCl) vs. a)  $pH$  and b) graphene mass percentage added with their correspondent error for all composites.

simplified Nernst equation for the redox reaction in question shown in Equation 4.1 representing the chemical equation [1] with a 4 electron pathway, where  $E$  is the non-standard cell potential,  $E^\circ$  is the standard cell potential,  $a$  is the activity of the specie and  $n$  is the number of electrons exchanged in the redox reaction.

$$E = E^\circ - \frac{RT}{nF} \ln \left( \frac{(a(H_2O))^2}{a(O_2) \cdot (a(H^+))^4} \right) \quad (4.1)$$

Equation 4.1 becomes equation 4.2 by considering the standard potential of the reduction of oxygen as 1.229 V, a temperature of 298 K and a four-electron mechanism, where water and oxygen, being pure phases, have an activity value of one.

$$E = 1.229 - \frac{0.0592}{4} \log \left( \frac{1}{a[H^+]^4} \right) \quad (4.2)$$

Using the definition of the  $pH$  (eq. 4.3), equation 4.2 becomes equation 4.4.

$$pH = -\log(a[H^+]) \quad (4.3)$$

$$E = 1.229 - \frac{0.0592}{4} \log \left( \frac{1}{10^{-4pH}} \right) \quad (4.4)$$

### 4.3. Catalytic Activity towards ORR

Finally, equation 4.5 shows the final linear relation between the potential and the  $pH$ .

$$E = 1.229 - 0.059 \cdot pH \quad (4.5)$$

When the medium possesses acidic  $pH$  and follows a 4 electron pathway, the potential will be higher and closer to the standard reduction potential, as long as the  $pH$  is elevated the potential will have lower values, which is the intended significance of the linear behavior expected shown in Figure 4.12 a). With a higher value of  $E$ , the better the electrocatalytic activity of the composite as the difference between the standard potential with the obtained potential is lower.

This relation between the onset potential and  $pH$  has been studied for different catalysts in the fields of energy conversion and storage<sup>70</sup>. In the case of the irregularity of the onset potential to increase as  $pH$  decreases shown in the systems, is important to consider the possibility of cations or anions which could be affecting the overall performance of the electrode, as these could be occupying the active sites required by oxygen to adsorb in the surface of the electrode. In the case of Pt, it has been found that certain adsorbed anions affect the kinetics of ORR by site blocking active sites<sup>71</sup>.

Fig. 4.12 b) shows, on the other side, the relation between the onset potential with the content of graphene. The tendency is clear, the onset potential values should become more positive when graphene is increased. This is because graphene provides an improvement in conductivity, electron transfer and reaction kinetics to the composite, making electrons to be conducted more efficiently from the circuit to the adsorbed oxygen, and allowing the reaction to start at higher potentials. However, not one composite showed a complete tendency to shift to more negative values of onset potential when the  $pH$  increased, or to go to more positive values of onset potential when the graphene amount increased at a single  $pH$ . Table 4.7 shows the values for the onset potentials and overpotentials of the composites as  $pH$  changes.

#### 4. Results and Discussion

Table 4.7.: Onset potential and overpotentials for all composites at different  $pH$ s.

	<b>Onset Potential (V) vs. Ag/AgCl <math>\pm</math> 0.03</b>			
<b><math>pH</math></b>	0.0% Gr. / 0.5% PVDF / 0.5% PVA	0.1% Gr. / 0.5% PVDF / 0.5% PVA	0.2% Gr. / 0.5% PVDF / 0.5% PVA	0.4% Gr. / 0.5% PVDF / 0.5% PVA
2	-0.31	-0.21	-0.16	-0.15
4	-0.38	-0.32	-0.25	-0.26
6	-0.46	-0.19	-0.34	-0.35
8	-0.43	-0.41	-0.28	-0.30
10	-0.44	-0.39	-0.24	-0.24
<b><math>pH</math></b>	<b>Overpotential (V) vs NHE</b>			
2	-1.20	-1.10	-1.05	-1.04
4	-1.15	-1.09	-1.02	-1.03
6	-1.12	-0.85	-1.00	-1.00
8	-0.97	-0.95	-0.82	-0.84
10	-0.86	-0.81	-0.66	-0.66

As stated before, the onset potential corresponds to the voltage in which reduction starts, and the current goes from nearly zero to lower values. For good catalytic performance, these values should be closer to the electrochemical equilibrium potential in which the oxygen reduction occurs at a given  $pH$ . The difference between the onset values and the  $E^\circ$  is known as overpotential ( $\eta$ ), and depends also on the  $pH$ . Composites with 0.2 and 0.4 wt% in graphene content show onset potentials of -0.16 V and -0.15 V against Ag/AgCl respectively at  $pH = 2$ . The possible explanation for the behavior of the composites to go to more positive values rather than to more negative in terms of onset potential when the  $pH$  is increased can be because of the active sites occupation by ions and not oxygen, making it harder for electrons to get to this oxygen and reduce it.

### 4.3. Catalytic Activity towards ORR

A comparison in the improvement percentage of the onset potential vs the graphene addition at every  $pH$  is shown in Figure 4.14, where, by comparing all the composites studied, it is noted that the reaction starts faster in the 0.4% composite, with the lowest values of overpotentials at every  $pH$ , as can be seen in Fig. 4.13. The red part shows the lower overpotentials of the composites at basic  $pH$ s and at the highest graphene composition. This result is explained by the lower standard reduction potential needed at basic  $pH$  to perform the reduction of oxygen.

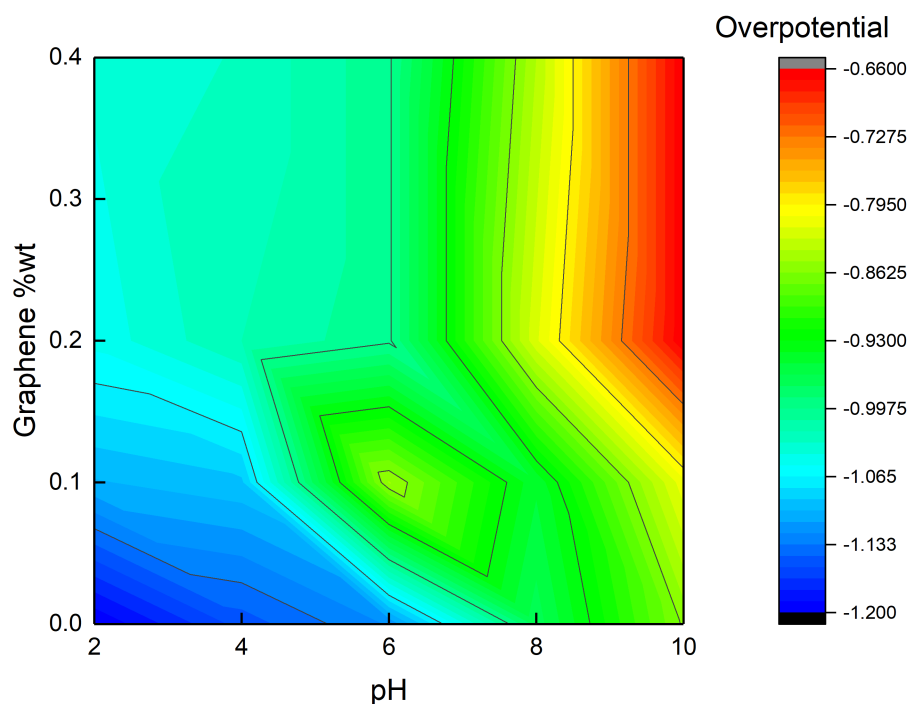


Figure 4.13.: Contour plot representing the relation between the  $pH$ , the graphene content and the overpotential of the composites.

These results present the 0.4 wt% composite as the one with the best performance in the study, confirmed by the EIS results in section 4.2.2. in which the impedance was the lowest, and that obtained in section 4.2.1. with higher peak currents and smaller potential peak separation. The onset potential result for the chosen 0.4 wt% graphene composite (0.07 V vs. NHE) is, however, twelve times lower when comparing it to

#### *4. Results and Discussion*

the Pt/C catalyst (0.88 V vs. NHE <sup>72</sup>) which is the commercial catalyst used for ORR, showing that the composite has not reached a comparable point to common catalysts. A possible approach to improve this will be to increase the concentration of all the compounds, knowing that both polymers work better at the same composition and that graphene should be added in at least a 1:5 ratio to that of the polymeric matrix.

### 4.3. Catalytic Activity towards ORR

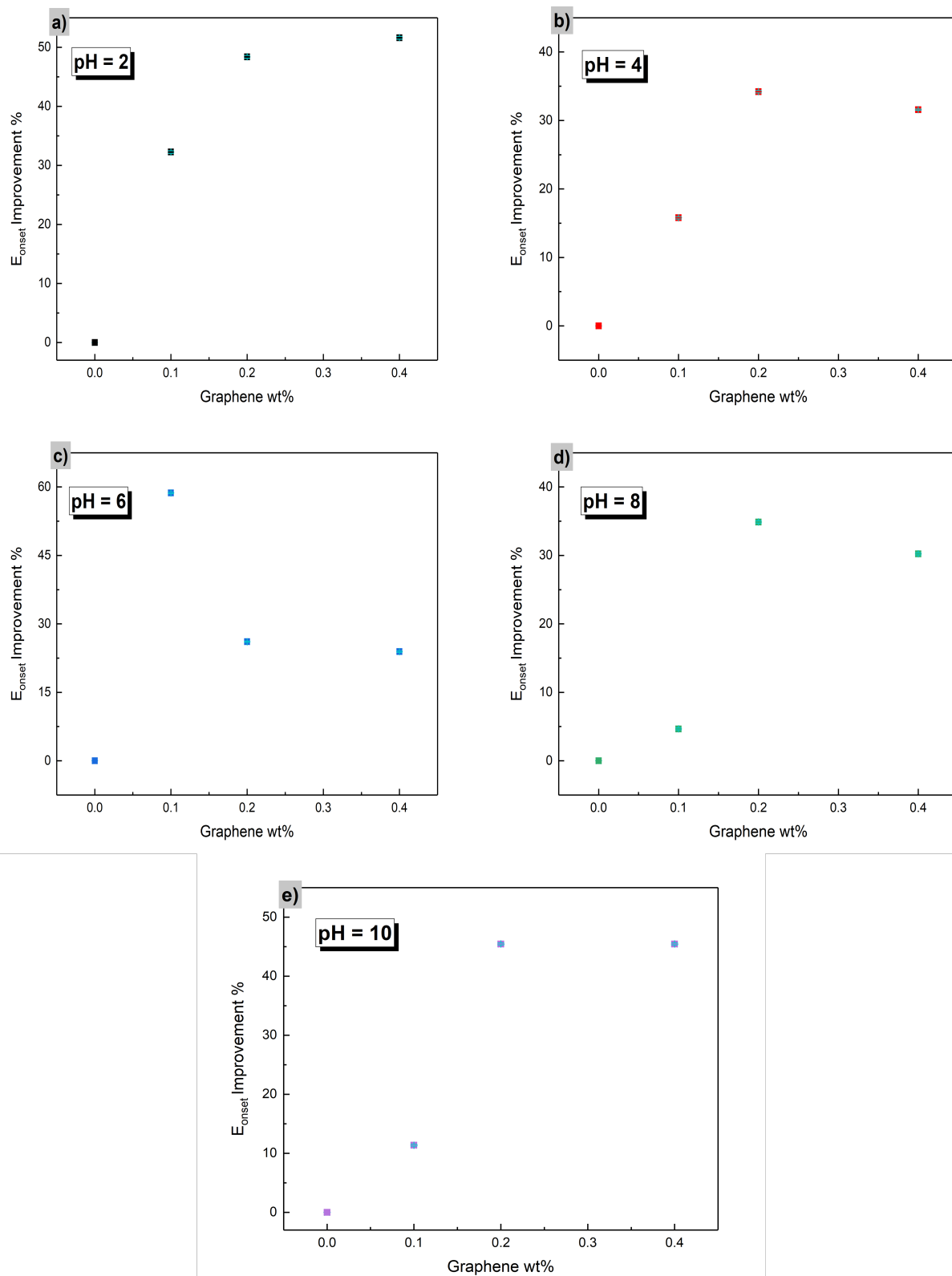


Figure 4.14.: Onset potential improvements in percentage vs. the graphene content at every *pH*.

## 5. Conclusion

Results showed the possibility to use a polymeric matrix formed by PVDF and PVA, both in 0.5 wt%, along with graphene, as electrodes in order to study their catalytic activity towards ORR. It was shown that PVDF by itself performs insufficiently and requires very large amounts of nanocarbon material as reported in the literature. Further addition of a second polymer, in this case PVA, improves the characteristics of the overall composite. PVA worked perfectly in this job and enhanced the cathodic current compared to the PVDF electrode. This mixture reached a cathodic peak current of  $-64.6 \mu\text{A}$  compared to the  $-19.8 \mu\text{A}$  of PVA and the lack of cathodic current generated by PVDF; and a peak potential separation of 0.21 V over a 0.53 V from PVA in the CV results, hinting at a better electrocatalytic performance of the polymer mixture compared to the PVDF and PVA electrodes.

Increasing the amount of PVDF in the overall composite showed to be detrimental to performance. Increasing the amount of PVA on the other side did not allow a good adhesion of the polymeric matrix. Increasing both polymers in the same proportion improved the composites' electrochemical behavior as it increases the current generated and lower the peak potential separation, making the composite with 0.5% PVDF / 0.5% PVA the chosen polymeric matrix.

After the addition of graphene to the matrix, the CV results in ferricyanide solution showed that the catalysts with the best performance were the 0.2 and 0.4 wt% graphene/polymeric matrix composite, with a cathodic peak current of  $-112 \mu\text{A}$  and  $-133 \mu\text{A}$  and a peak potential separation of 0.22 V and 0.17 V respectively. All graphene composites had higher peak currents than the polymeric matrix, increasing by a factor of 1.8 to 2.1, respectively. The current response showed little increase for graphene

above 0.2 wt%.

EIS measurements were also performed in order to know more about the behavior of the electrode/electrolyte system. Results showed that the charge transfer resistance was lowest when using the 0.4% graphene composite with an obtained value of 468.5  $\Omega$ , value that is 4.7 times lower than that of the polymer matrix. Diffusion was the greatest contributor to the system's impedance. This results showed no saturation in the graphene compounds like the CV results, with higher values for the two first graphene addition and then a decrease in the impedance.

The evaluation of the catalytic performance of the composites towards ORR was studied by CVs and evaluated at different *pH*. This study corroborates the results obtained by CVs in the ferricyanide solution, as graphene was added. The highest onset potential was for 0.4% graphene composite with -0.15 V at *pH* = 2, and -0.24 at *pH* = 10. In general, for all composites, acidic *pH*s showed better results regarding the onset potentials, but basic *pH*s presented the lowest overpotentials, which resulted in lower values for the 0.4% composite with -0.66 V vs. NHE at *pH* = 10, which is 1.3 times better than the -1.2 V result that the polymeric matrix shows.

Even though the cost-benefits relation between the 0.2 and the 0.4 wt% composites was favorable to the first mentioned composite in the CV in ferricyanide solution, results in both EIS and CV in air saturated solution showed better results for the second composite. The 0.4 wt% composite showed the best results in every electrochemical probe, with the highest peak currents, lowest peak potential separation, lowest impedance and charge transfer resistance, and the lowest overpotentials at every *pH*, showing the best electrocatalytic activity towards ORR.

Further research must be performed in order to understand more about the pathway of reduction in the electrode surface, with rotating disk electrode, or rotating ring disk electrode measurements to obtain the number of electrons exchanged in the reaction using the studied composite. SEM or TEM images will be also useful to understand

the active sites available for oxygen to adsorb, and to see the link between it and the catalytic performance of the compound. In this way, a composition and ratio in which the catalyst improves the overpotential results could be obtained.

# A. Appendix

## A.1. List of Abbreviations

AC	Activated Carbon
CNTs	Carbon Nanotubes
CPE	Constant Phase Element
CV	Cyclic Voltammetry
DMA	Dimethylacetamide
DMSO	Dimethyl Sulfoxide
EIS	Electrochemical Impedance Spectroscopy
GC	Glassy Carbon
MFCs	Microbial Fuel Cell
NHE	Normal Hydrogen Electrode
OER	Oxygen Evolution Reaction
ORR	Oxygen Reduction Reaction
PBS	Phosphate Buffer Solution
PEM	Proton Exchange Membrane
PVA	Polyvinyl Alcohol
PVDF	Polyvinylidene Fluoride

## A.2. Scientific Output

Parts of this thesis were published in:

- Poster presentation at CMD2020GEFES international conference, organized by the Spanish Royal Physics Society (RSEF-GEFES) and the European Physical Society (EPS-CMD), from August 31 to September 4, 2020.
- "Few Layers Graphene Nanoplatelets-Based Composite Electrodes for Improved Oxygen Reduction Reaction Electrocatalytic Activity", manuscript in preparation.

# Bibliography

- [1] Logan, B. E. *Microbial Fuel Cells*; John Wiley & Sons, 2008. <https://doi.org/10.1016/B978-0-444-53199-5.00098-1>.
- [2] Ci, S.; Cai, P.; Wen, Z.; Li, J. Graphene-Based Electrode Materials for Microbial Fuel Cells. *Sci. China Mater.* **2015**, *58* (6), 496–509. <https://doi.org/10.1007/s40843-015-0061-2>.
- [3] Cheng, S.; Liu, H.; Logan, B. E. Power Densities Using Different Cathode Catalysts (Pt and CoTMPP) and Polymer Binders (Nafion and PTFE) in Single Chamber Microbial Fuel Cells. *Environ. Sci. Technol.* **2006**, *40* (1), 364–369.
- [4] Gautam, R. K.; Verma, A. *Electrocatalyst Materials for Oxygen Reduction Reaction in Microbial Fuel Cell*; Elsevier B.V., 2019. <https://doi.org/10.1016/B978-0-444-64052-9.00018-2>.
- [5] Wang, X.; Li, Z.; Qu, Y.; Yuan, T.; Wang, W.; Wu, Y. Review of Metal Catalysts for Oxygen Reduction Reaction: From Nanoscale Engineering to Atomic Design. *CHEMPR* **2019**, 1–26. <https://doi.org/10.1016/j.chempr.2019.03.002>.
- [6] Zhao, F.; Harnisch, F.; Schröder, U.; Scholz, F.; Bogdanoff, P.; Herrmann, I. Application of Pyrolysed Iron(II) Phthalocyanine and CoTMPP Based Oxygen Reduction Catalysts as Cathode Materials in Microbial Fuel Cells. *Electrochem. commun.* **2005**, *7* (12), 1405–1410. <https://doi.org/10.1016/j.elecom.2005.09.032>.
- [7] Cui, L.; Cui, L.; Li, Z.; Zhang, J.; Wang, H.; Lu, S.; Xiang, Y. A Copper Single-Atom Catalyst towards Efficient and Durable Oxygen Reduction for Fuel Cells. *J. Mater. Chem. A* **2019**, *7* (28), 16690–16695. <https://doi.org/10.1039/c9ta03518d>.
- [8] Li, F.; Han, G. F.; Noh, H. J.; Kim, S. J.; Lu, Y.; Jeong, H. Y.; Fu, Z.; Baek, J. B. Boosting Oxygen Reduction Catalysis with Abundant Copper Single Atom Active Sites. *Energy Environ. Sci.* **2018**, *11* (8), 2263–2269. <https://doi.org/10.1039/c8ee01169a>.
- [9] Wu, J.; Yang, R.; Yan, W. Phosphorus-Doped Hierarchical Porous Carbon as Efficient Metal-Free Electrocatalysts for Oxygen Reduction Reaction. *Int. J. Hydrogen Energy* **2019**, *44* (26), 12941–12951. <https://doi.org/10.1016/j.ijhydene.2019.02.094>.
- [10] Jha, S.; Bhandary, N.; Basu, S.; Ingole, P. P. Electro-Deposited Pt<sub>3</sub>Co on Carbon Fiber Paper as Nafion-Free Electrode for Enhanced Electro-Catalytic Activity toward Oxygen Reduction Reaction. *ACS Appl. Energy Mater.* **2019**, *2* (9), 6269–6279. <https://doi.org/10.1021/acsaem.9b00849>.

- [11] Araújo, M. P.; Nunes, M.; Rocha, I. M.; Pereira, M. F. R.; Freire, C. Electrocatalytic Activity of New Mn<sub>3</sub>O<sub>4</sub> @oxidized Graphene Flakes Nanocomposites toward Oxygen Reduction Reaction. *J. Mater. Sci.* **2019**, *54* (12), 8919–8940. <https://doi.org/10.1007/s10853-019-03508-6>.
- [12] Sui, S.; Wang, X.; Zhou, X.; Su, Y.; Riffat, S.; Liu, C. jun. A Comprehensive Review of Pt Electrocatalysts for the Oxygen Reduction Reaction: Nanostructure, Activity, Mechanism and Carbon Support in PEM Fuel Cells. *J. Mater. Chem. A* **2017**, *5* (5), 1808–1825. <https://doi.org/10.1039/C6TA08580F>.
- [13] Tsai, H. Y.; Hsu, W. H.; Liao, Y. J. Effect of Electrode Coating with Graphene Suspension on Power Generation of Microbial Fuel Cells. *Coatings* **2018**, *8* (7). <https://doi.org/10.3390/coatings8070243>.
- [14] Zhou, R.; Zheng, Y.; Jaroniec, M.; Qiao, S. Z. Determination of the Electron Transfer Number for the Oxygen Reduction Reaction: From Theory to Experiment. *ACS Catal.* **2016**, *6* (7), 4720–4728. <https://doi.org/10.1021/acscatal.6b01581>.
- [15] Jiao, Y.; Zheng, Y.; Jaroniec, M.; Qiao, S. Z. Origin of the Electrocatalytic Oxygen Reduction Activity of Graphene-Based Catalysts: A Roadmap to Achieve the Best Performance. *J. Am. Chem. Soc.* **2014**, *136* (11), 4394–4403. <https://doi.org/10.1021/ja500432h>.
- [16] Song, C.; Zhang, J. Electrocatalytic Oxygen Reduction Reaction. In *PEM Fuel Cell Electrocatalysts and Catalyst Layers: Fundamentals and Applications*; Springer London: London, 2008; 89–134. [https://doi.org/10.1007/978-1-84800-936-3\\_2](https://doi.org/10.1007/978-1-84800-936-3_2).
- [17] Li, Y.; Li, Q.; Wang, H.; Zhang, L.; Wilkinson, D. P.; Zhang, J. Recent Progresses in Oxygen Reduction Reaction Electrocatalysts for Electrochemical Energy Applications. *Electrochem. Energy Rev.* **2019**, *2* (4), 518–538. <https://doi.org/10.1007/s41918-019-00052-4>.
- [18] Khotseng, L. Oxygen Reduction Reaction. In *Electrocatalysts for Fuel Cells and Hydrogen Evolution - Theory to Design*; IntechOpen, 2018; 25–50. <https://doi.org/10.5772/intechopen.79098>.
- [19] Slate, A. J.; Whitehead, K. A.; Brownson, D. A. C.; Banks, C. E. Microbial Fuel Cells: An Overview of Current Technology. *Renew. Sustain. Energy Rev.* **2019**, *101*, 60–81. <https://doi.org/10.1016/j.rser.2018.09.044>.
- [20] Nørskov, J. K.; Rossmeisl, J.; Logadottir, A.; Lindqvist, L.; Kitchin, J. R.; Bligaard, T.; Jónsson, H. Origin of the Overpotential for Oxygen Reduction at a Fuel-Cell Cathode. *J. Phys. Chem. B* **2004**, *108* (46), 17886–17892. <https://doi.org/10.1021/jp047349j>.
- [21] Shao, M.; Chang, Q.; Dodelet, J. P.; Chenitz, R. Recent Advances in Electrocatalysts for Oxygen Reduction Reaction. *Chem. Rev.*, **2016**, 3594–3657. <https://doi.org/10.1021/acs.chemrev.5b00462>.

- [22] Stamenkovic, V. R.; Mun, B. S.; Arenz, M.; Mayrhofer, K. J. J.; Lucas, C. A.; Wang, G.; Ross, P. N.; Markovic, N. M. Trends in Electrocatalysis on Extended and Nanoscale Pt-Bimetallic Alloy Surfaces. *Nat. Mater.* **2007**, *6* (3), 241–247. <https://doi.org/10.1038/nmat1840>.
- [23] Stamenkovic, V. R.; Fowler, B.; Mun, B. S.; Wang, G.; Ross, P. N.; Lucas, C. A.; Markovic, N. M. Improved Oxygen Reduction Activity on Pt<sub>3</sub>Ni(111) via Increased Surface Site Availability. *Science* **2007**, *315* (5811), 493–497. <https://doi.org/10.1126/science.1135941>.
- [24] Zhang, L.; Liu, C.; Zhuang, L.; Li, W.; Zhou, S.; Zhang, J. Manganese Dioxide as an Alternative Cathodic Catalyst to Platinum in Microbial Fuel Cells. *Biosens. Bioelectron.* **2009**, *24* (9), 2825–2829. <https://doi.org/10.1016/j.bios.2009.02.010>.
- [25] Wen, Q.; Wang, S.; Yan, J.; Cong, L.; Pan, Z.; Ren, Y.; Fan, Z. MnO<sub>2</sub>-Graphene Hybrid as an Alternative Cathodic Catalyst to Platinum in Microbial Fuel Cells. *J. Power Sources* **2012**, *216*, 187–191. <https://doi.org/10.1016/j.jpowsour.2012.05.023>.
- [26] Cha, C.; Shin, S. R.; Annabi, N.; Dokmeci, M. R.; Khademhosseini, A. Carbon-Based Nanomaterials: Multifunctional Materials for Biomedical Engineering. *ACS Nano*. NIH Public Access April 23, 2013, 2891–2897. <https://doi.org/10.1021/nn401196a>.
- [27] Saito, R.; Dresselhaus, G.; Dresselhaus, M. S. *Physical Properties of Carbon Nanotubes*; Published by Imperial College Press and distributed by World Scientific Publishing CO., 1998. <https://doi.org/10.1142/p080>.
- [28] Yamamoto, T.; Watanabe, K.; Hernández, E. R. Mechanical Properties, Thermal Stability and Heat Transport in Carbon Nanotubes. In *Carbon Nanotubes: Advanced Topics in the Synthesis, Structure, Properties and Applications*; 2007; Vol. 111, 165–194. [https://doi.org/10.1007/978-3-540-72865-8\\_5](https://doi.org/10.1007/978-3-540-72865-8_5).
- [29] Endo, M.; Strano, M. S.; Ajayan, P. M. Potential Applications of Carbon Nanotubes. In *Carbon Nanotubes: Advanced Topics in the Synthesis, Structure, Properties and Applications*; 2007; Vol. 111, p 61. [https://doi.org/10.1007/978-3-540-72865-8\\_2](https://doi.org/10.1007/978-3-540-72865-8_2).
- [30] Tadda, M. A.; Ahsan, A.; Shitu, A.; ElSergany, M.; Arunkumar, T.; Jose, B.; Razaque, M. A.; Nik Daud, N. N. A Review on Activated Carbon: Process, Application and Prospects. *J. Adv. Civ. Eng. Pract. Res.* **2016**, *2* (1), 7–13.
- [31] Lee, X. J.; Hiew, B. Y. Z.; Lai, K. C.; Lee, L. Y.; Gan, S.; Thangalazhy-Gopakumar, S.; Rigby, S. Review on Graphene and Its Derivatives: Synthesis Methods and Potential Industrial Implementation. *J. Taiwan Inst. Chem. Eng.* **2019**, *98*, 163–180. <https://doi.org/10.1016/j.jtice.2018.10.028>.

- [32] Meyer, J. C.; Geim, A. K.; Katsnelson, M. I.; Novoselov, K. S.; Booth, T. J.; Roth, S. The Structure of Suspended Graphene Sheets. *Nature* **2007**, *446* (7131), 60–63. <https://doi.org/10.1038/nature05545>.
- [33] Ren, S.; Rong, P.; Yu, Q. Preparations, Properties and Applications of Graphene in Functional Devices: A Concise Review. *Ceram. Int.* **2018**, *44* (11), 11940–11955. <https://doi.org/10.1016/j.ceramint.2018.04.089>.
- [34] Geim, A. K. Graphene: Status and Prospects. *Science* **2009**, *324* (June), 1530–1535. <https://doi.org/10.1126/science.1158877>.
- [35] Zhen, Z.; Zhu, H. *Structure and Properties of Graphene*; Elsevier Inc., 2018. <https://doi.org/10.1016/b978-0-12-812651-6.00001-x>.
- [36] D. Ghuge, A.; R. Shirode, A.; J. Kadam, V. Graphene: A Comprehensive Review. *Curr. Drug Targets* **2017**, *18* (6), 724–733. <https://doi.org/10.2174/1389450117666160709023425>.
- [37] Yan, Z.; Wang, M.; Huang, B.; Liu, R. Graphene Supported Pt-Co Alloy Nanoparticles as Cathode Catalyst for Microbial Fuel Cells *Int. J. Electrochem. Sci.* **2013**, (8), 149–158.
- [38] Najafpour, G. D. Microbial Fuel Cells: A New Source of Power. In *Biochemical Engineering and Biotechnology*. Elsevier: 2015; pp 527–555. <https://doi.org/10.1016/B978-0-444-63357-6.00018-3>.
- [39] Wang, H. F.; Xu, Q. Materials Design for Rechargeable Metal-Air Batteries. *Matter* **2019**, *1* (3), 565–595. <https://doi.org/10.1016/j.matt.2019.05.008>.
- [40] Girishkumar, G.; McCloskey, B.; Luntz, A. C.; Swanson, S.; Wilcke, W. Lithium-Air Battery: Promise and Challenges. *J. Phys. Chem. Lett.* **2010**, *1* (14), 2193–2203. <https://doi.org/10.1021/jz1005384>.
- [41] Chawla, N. Recent Advances in Air-Battery Chemistries. *Mater. Today Chem.* **2019**, *12*, 324–331. <https://doi.org/10.1016/j.mtchem.2019.03.006>.
- [42] Wang, H. F.; Tang, C.; Zhang, Q. A Review of Precious-Metal-Free Bifunctional Oxygen Electrocatalysts: Rational Design and Applications in Zn–Air Batteries. *Adv. Funct. Mater.* **2018**, *28* (46), 1803329. <https://doi.org/10.1002/adfm.201803329>.
- [43] Lyon, L. A.; Keating, C. D.; Fox, A. P.; Baker, B. E.; He, L.; Nicewarner, S. R.; Mulvaney, S. P.; Natan, M. J. Raman Spectroscopy. *Anal. Chem.* **1998**, *70* (12), 341–362. <https://doi.org/10.1021/a1980021p>.
- [44] Ferraro, J. R.; Nakamoto, K.; Brown, C. W. *Introductory Raman Spectroscopy: Second Edition*; Elsevier Inc., 2003. <https://doi.org/10.1016/B978-0-12-254105-6.X5000-8>.

- [45] Elgrishi, N. N.; Rountree, K. J.; Mccarthy, B. D.; Rountree, E. S.; Eisenhart, T. T.; Dempsey, J. L. A Practical Beginner's Guide to Cyclic Voltammetry. **2017**. <https://doi.org/10.1021/acs.jchemed.7b00361>.
- [46] Kissinger, P. T.; Heineman, W. R. Cyclic Voltammetry. *J. Chem. Educ.* **1983**, 702–706. <https://doi.org/10.1021/ed060p702>.
- [47] Zahn, R.; Coullerez, G.; Vörös, J.; Zambelli, T. Effect of Polyelectrolyte Interdiffusion on Electron Transport in Redox-Active Polyelectrolyte Multilayers. *J. Mater. Chem.* **2012**, 22, 11073–11078. <https://doi.org/10.1039/c2jm30469d>.
- [48] Li, S.; Thomas, A. Emerged Carbon Nanomaterials from Metal-Organic Precursors for Electrochemical Catalysis in Energy Conversion. In *Advanced Nanomaterials for Electrochemical-Based Energy Conversion and Storage*; Elsevier, 2019; 393–423. <https://doi.org/10.1016/b978-0-12-814558-6.00012-5>.
- [49] Liang, H. W.; Zhuang, X.; Brüller, S.; Feng, X.; Müllen, K. Hierarchically Porous Carbons with Optimized Nitrogen Doping as Highly Active Electrocatalysts for Oxygen Reduction. *Nat. Commun.* **2014**, 5 (May), 1–7. <https://doi.org/10.1038/ncomms5973>.
- [50] Tahir, M.; Pan, L.; Idrees, F.; Zhang, X.; Wang, L.; Zou, J. J.; Wang, Z. L. Electrocatalytic Oxygen Evolution Reaction for Energy Conversion and Storage: A Comprehensive Review. *Nano Energy* **2017**, 37, 136–157. <https://doi.org/10.1016/j.nanoen.2017.05.022>.
- [51] Gamry Instruments. Basics of EIS: Electrochemical Research-Impedance <https://www.gamry.com/application-notes/EIS/basics-of-electrochemical-impedance-spectroscopy/> (accessed Dec 18, 2019).
- [52] Barsoukov, E.; Macdonald, J. R. *Impedance Spectroscopy Theory, Experiments and Applications*; Wiley-Interscience, 2005; Vol. 125.
- [53] Monk, P. M. S. *Fundamentals of Electroanalytical Chemistry*; Wiley, 2001.
- [54] Kuang, F.; Zhang, D.; Li, Y.; Wan, Y.; Hou, B. Electrochemical Impedance Spectroscopy Analysis for Oxygen Reduction Reaction in 3.5% NaCl Solution. *J. Solid State Electrochem.* **2009**, 13 (3), 385–390. <https://doi.org/10.1007/s10008-008-0570-y>.
- [55] Wagner, N.; Friedrich, K. A. Application of Electrochemical Impedance Spectroscopy for Fuel Cell Characterization: PEFC and Oxygen Reduction Reaction in Alkaline Solution. *Fuel Cells* **2009**, 9 (3), 237–246. <https://doi.org/10.1002/fuce.200800071>.
- [56] Chapman, S. J.; Hewett, D. P.; Trefethen, L. N. Mathematics of the Faraday Cage. *SIAM Rev.* **2015**, 57 (3), 398–417. <https://doi.org/10.1137/140984452>.

- [57] Riosbaas, M. T.; Loh, K. J.; O'Bryan, G.; Loyola, B. R. In Situ Phase Change Characterization of PVDF Thin Films Using Raman Spectroscopy. In *Sensors and Smart Structures Technologies for Civil, Mechanical, and Aerospace Systems 2014*; Lynch, J. P., Wang, K.-W., Sohn, H., Eds.; SPIE, 2014; Vol. 9061, p 90610Z. <https://doi.org/10.1117/12.2045430>.
- [58] Constantino, C. J. L.; Job, A. E.; Simoes, R. D.; Giacometti, J. A.; Zucolotto, V.; Oliveira, O. N.; Gozzi, G.; Chinaglia, D. L. The Investigation of Alpha-Beta Phase Transition in Poly(Vinylidene Fluoride) (PVDF). In *2005 12th International Symposium on Electrets; IEEE*; 178–181. <https://doi.org/10.1109/ISE.2005.1612350>.
- [59] Ji, Y.; Liu, J.; Jiang, Y.; Liu, Y. Analysis of Raman and Infrared Spectra of Poly(Vinylidene Fluoride) Irradiated by KrF Excimer Laser. *Spectrochim. Acta - Part A Mol. Biomol. Spectrosc.* **2008**, *70* (2), 297–300. <https://doi.org/10.1016/j.saa.2007.07.061>.
- [60] Marka, S. K.; Sindam, B.; James Raju, K. C.; Srikanth, V. V. S. S. Flexible Few-Layered Graphene/Poly Vinyl Alcohol Composite Sheets: Synthesis, Characterization and EMI Shielding in X-Band through the Absorption Mechanism. *RSC Adv.* **2015**, *5* (46), 36498–36506. <https://doi.org/10.1039/c5ra04038h>.
- [61] Tang, B.; Guoxin, H.; Gao, H. Raman Spectroscopic Characterization of Graphene. *Appl. Spectrosc. Rev.* **2010**, *45* (5), 369–407. <https://doi.org/10.1080/05704928.2010.483886>.
- [62] Shi, L. PVDF-Graphene conductive composite membrane and PVA-Graphene conductive composite membrane preparation and application, University of Delaware, 2014.
- [63] Yang, W.; He, W.; Zhang, F.; Hickner, M. A.; Logan, B. E. Single-Step Fabrication Using a Phase Inversion Method of Poly(Vinylidene Fluoride) (PVDF) Activated Carbon Air Cathodes for Microbial Fuel Cells. *Environ. Sci. Technol. Lett.* **2014**, *1* (10), 416–420. <https://doi.org/10.1021/ez5002769>.
- [64] Ningaraju, S.; Ravikumar, H. B. Studies on Electrical Conductivity of PVA/Graphite Oxide Nanocomposites: A Free Volume Approach. *J. Polym. Res.* **2016**, *24* (1), 1–11. <https://doi.org/10.1007/s10965-016-1176-1>.
- [65] Isawi, H. Evaluating the Performance of Different Nano-Enhanced Ultrafiltration Membranes for the Removal of Organic Pollutants from Wastewater. *J. Water Process Eng.* **2019**, *31*, 1–15. <https://doi.org/10.1016/j.jwpe.2019.100833>.
- [66] Razmgar, K.; Saljoughi, E.; Mousavi, S. M. Preparation and Characterization of a Novel Hydrophilic PVDF/PVA/Al<sub>2</sub>O<sub>3</sub> Nanocomposite Membrane for Removal of As(V) from Aqueous Solutions. *Polym. Compos.* **2018**, *40* (1), 2452–2461. <https://doi.org/10.1002/pc.25115>.

- [67] Nicholson, R. S.; Shain, I. Theory of Stationary Electrode Polarography: Single Scan and Cyclic Methods Applied to Reversible, Irreversible, and Kinetic Systems. *Anal. Chem.* **1964**, *36* (4), 706–723. <https://doi.org/10.1021/ac60210a007>.
- [68] Morales, U. P.; López, E. V.; Ojalora, C. O. Aspectos Básicos En La Interpretación de Diagramas de Impedancia Electroquímica. *DYNA* **2010**, *77* (162), 13–19.
- [69] Yang, Z.; Yao, Z.; Li, G.; Fang, G.; Nie, H.; Liu, Z.; Zhou, X.; Chen, X.; Huang, S. Sulfur-Doped Graphene as an Efficient Metal-Free Cathode Catalyst for Oxygen Reduction. *ACS Nano* **2012**, *6* (1), 205–211. <https://doi.org/10.1021/nn203393d>.
- [70] Duan, Z.; Henkelman, G. Calculations of the PH-Dependent Onset Potential for CO Electrooxidation on Au(111). *Langmuir* **2018**, *34* (50), 15268–15275. <https://doi.org/10.1021/acs.langmuir.8b03644>.
- [71] Jusys, Z.; Behm, R. J. The Effect of Anions and PH on the Activity and Selectivity of an Annealed Polycrystalline Au Film Electrode in the Oxygen Reduction Reaction-Revisited. *ChemPhysChem* **2019**, *20* (24), 3276–3288. <https://doi.org/10.1002/cphc.201900960>.
- [72] Wang, Y.; Song, S.; Maragou, V.; Shen, P. K.; Tsiakaras, P. High Surface Area Tungsten Carbide Microspheres as Effective Pt Catalyst Support for Oxygen Reduction Reaction. *Appl. Catal. B Environ.* **2009**, *89* (1–2), 223–228. <https://doi.org/10.1016/j.apcatb.2008.11.032>.